



**HAL**  
open science

# Postcrania of *Borealestes* (Mammaliformes, Docodonta) and the emergence of ecomorphological diversity in early mammals

Elsa Panciroli, Roger B. J. Benson, Vincent Fernandez, Matthew Humpage, Alberto Martin-Serra, Stig Walsh, Zhe-Xi Luo, Nicholas C. Fraser

## ► To cite this version:

Elsa Panciroli, Roger B. J. Benson, Vincent Fernandez, Matthew Humpage, Alberto Martin-Serra, et al.. Postcrania of *Borealestes* (Mammaliformes, Docodonta) and the emergence of ecomorphological diversity in early mammals. *Palaeontology*, 2022, 65 (1), pp.e12577-1-e12577-36. 10.1111/pala.12577 . hal-03722396

**HAL Id: hal-03722396**

**<https://hal.science/hal-03722396>**








Submitted on 13 Jul 2022

**HAL** is a multi-disciplinary open access archive for the deposit and dissemination of scientific research documents, whether they are published or not. The documents may come from teaching and research institutions in France or abroad, or from public or private research centers.

L'archive ouverte pluridisciplinaire **HAL**, est destinée au dépôt et à la diffusion de documents scientifiques de niveau recherche, publiés ou non, émanant des établissements d'enseignement et de recherche français ou étrangers, des laboratoires publics ou privés.



# POSTCRANIA OF *BOREALESTES* (MAMMALIFORMES, DOCODONTA) AND THE EMERGENCE OF ECOMORPHOLOGICAL DIVERSITY IN EARLY MAMMALS

by ELSA PANCIROLI<sup>1,2,3</sup> , ROGER B.J. BENSON<sup>4</sup> ,  
VINCENT FERNANDEZ<sup>5,6</sup> , MATTHEW HUMPAGE<sup>1</sup>,  
ALBERTO MARTÍN-SERRA<sup>7</sup> , STIG WALSH<sup>2,3</sup> , ZHE-XI LUO<sup>8</sup>  and  
NICHOLAS C. FRASER<sup>2,3</sup> 

<sup>1</sup>Oxford University Museum of Natural History, Oxford OX1 3PW, UK; [elsa.panciroli@oum.ox.ac.uk](mailto:elsa.panciroli@oum.ox.ac.uk)

<sup>2</sup>Natural Sciences Department, National Museums Scotland, Edinburgh EH1 1JF, UK

<sup>3</sup>School of Geosciences, Grant Institute, University of Edinburgh, Edinburgh EH9 3JW, UK

<sup>4</sup>Department of Earth Sciences, University of Oxford, Oxford OX1 3AN, UK

<sup>5</sup>European Synchrotron Radiation Facility (ESRF), Beamline ID19, Grenoble, France

<sup>6</sup>Natural History Museum, Cromwell Road, London SW7 5BD, UK

<sup>7</sup>Departamento de Ecología y Geología, Facultad de Ciencias, Universidad de Málaga, Campus de Teatinos s/n, 20971 Málaga, Spain

<sup>8</sup>Department of Organismal Biology and Anatomy, The University of Chicago, Chicago, IL, USA

Typescript received 10 March 2021; accepted in revised form 15 July 2021

**Abstract:** The Middle Jurassic witnessed the early diversification of mammal groups, including the stem-mammalian clade, Docodonta. Recent discoveries in China indicate docodontans exhibited ecomorphological diversity akin to small-bodied mammals living >100 million years later, in the Cenozoic. Our understanding of the emergence of this ecological diversity is hindered by a lack of Middle Jurassic fossil material from other parts of the world. The two partial postcranial skeletons of *Borealestes* described here come from the Kilmaluag Formation, Scotland. These are the most complete Mesozoic mammaliaform skeletons currently known from the UK, and among the best preserved in Europe. As an early member of Docodonta, *Borealestes* provides key anatomical information for understanding the clade's evolution, and the emergence of mammaliaform ecomorphological diversity. Using digital reconstructions from micro-CT and synchrotron scans, we describe the postcranial anatomy of *Borealestes* and provide an updated phylogenetic analysis

incorporating cranial and postcranial characters. We find *Borealestes* species form a sister group to a clade comprising *Agilodocodon* and *Microdocodon*. To complement observational analyses of the skeleton, we carry out principal components analyses using 3D landmarks on a comparative dataset of 42 extant mammal taxa. Our results indicate *Borealestes* lacked specializations for derived locomotor behaviour. We detect some similarity in the humerus between *Borealestes* and *Ornithorhynchus*. *Borealestes* is morphologically intermediate between the robust morphology of fossorial and semi-fossorial/semi-aquatic *Haldanodon* and *Docofossor*, and the gracile morphology for scansorial *Agilodocodon* and *Microdocodon*. We suggest ecological diversity in Docodonta may arise from an unspecialized basal bauplan, of which *Borealestes* may be representative.

**Key words:** mammal, Middle Jurassic, ecomorphology, Bathonian, geometric morphometrics.

ONE of the most exciting developments in Mesozoic mammal palaeontology in the last 15 years has been the unexpected discovery of high ecological diversity in Jurassic docodontans. Their divergent ecologies include fossorial, semi-aquatic and arboreal specializations (Martin 2005; Ji *et al.* 2006; Luo *et al.* 2015a; Meng *et al.* 2015; Zhou *et al.* 2019). Docodonta comprise one of the earliest branches of Mammaliaformes (*sensu* Rowe 1988; Luo 2007), and therefore are a key group for informing our

understanding of mammal macroevolution, and the emergence of ecomorphological diversity in early Mesozoic mammaliaforms as a whole. However, a lack of postcranial material for more basal docodontan genera means we currently know little about how this ecomorphological diversity first emerged in this clade, or to what extent it contributed to their overall morphological disparity.

Docodonta were initially identified from mandibular and dental remains, demonstrating unusually complex

tooth morphologies for early mammaliaforms (Simpson 1929; Jenkins 1969; Gingerich 1973; Butler 1997). The first docodontan for which extensive cranial and postcranial material was known was *Haldanodon exspectatus*, from the Upper Jurassic of Portugal (Kühne & Krusat 1972; Lillegraven & Krusat 1991; Martin 2005). *Haldanodon* exhibits adaptations for a semi-fossorial and/or semi-aquatic lifestyle, with short, robust limb bones, and robust and mediolaterally wide phalanges, a pronounced deltopectoral crest and expanded distal joint of the humerus (Martin 2005). After this discovery, the Chinese docodontan, *Castoroocauda lustrasimilis* (Ji *et al.* 2006), from the upper Middle Jurassic, was found to have adaptations similar to that of the modern beaver or otter. Preserved soft tissue impressions indicate a wide and flattened tail with expanded double transverse processes on wide caudal vertebrae to support it (Ji *et al.* 2006). Soft tissue impressions around the hind feet suggest webbing between the digits, and its teeth are slightly recurved, perhaps facilitating a diet of aquatic invertebrates or even small fish (Ji *et al.* 2006). Such specializations were hitherto unknown in Mesozoic mammals. *Castoroocauda*'s plated ribs, a homoplastic feature among cynodonts that strengthens the trunk (Jenkins 1971), may be related to digging. Today, a semi-aquatic, semi-fossorial lifestyle of this kind is seen in the platypus, *Ornithorhynchus anatinus* (Fish 2000; Gambaryan *et al.* 2002).

*Agilodocodon scansorius*, also from the Middle Jurassic of China, exhibits adaptations for an arboreal lifestyle (Meng *et al.* 2015), as does *Microdocodon* (Zhou *et al.* 2019). These taxa are more gracile than other docodontans, with elongate proportions of the manus and pes similar to modern scansorial and arboreal mammals such as arboreal diprotodontan marsupials, or placental tree shrews (Meng *et al.* 2015). Unlike other docodontans and most early mammaliaforms, *Agilodocodon* has a relatively longer lumbar vertebral region that is rib-less, allowing a wider range of movement in the posterior vertebral column and probably facilitating dexterous body movements among branches (Gabe *et al.* 1967; Meng *et al.* 2015).

*Docofossor brachydactylus*, from the Middle Jurassic of China exhibits clear adaptations for a fossorial, most likely subterranean, lifestyle (Luo *et al.* 2015a). The teeth are simplified compared to other docodontans, the olecranon process is hypertrophied, and a trochleate astragalus allows for habitual abduction of the foot. The robust appendicular skeleton shows proportionally short limbs and reductions in digit segments caused by symphalangism: fusion of proximal and intermediate phalanges (Luo *et al.* 2015a). Such brachydactyly is seen in modern subterranean digging specialists such as the golden moles (Chrysochloridae) resulting in a short and widened manus perfect for removing and moving soil substrate (Kindahl 1949; Hildebrand 1985; Luo *et al.* 2015a).

Although they share some morphological features with the earliest mammaliaforms of the Late Triassic and Early Jurassic, such as *Morganucodon* (Hopson & Crompton 1969; Jenkins & Parrington 1976; Kermack *et al.* 1981), it is now clear that Docodonta exhibit an unusual amount of within-clade ecological diversity, approaching that seen among small-bodied extant therian mammals. It has been hypothesized that the molar complexity of docodontans may be a key factor in their ability to exploit new niche-space and diversify in dietary ecology (Luo & Martin 2007; Luo 2007; Meng *et al.* 2015). Because of their early divergence from other mammaliaforms, the postcranial morphology of docodontans can provide key information for understanding the morphological evolution of mammals as a whole (Simpson 1929; Lillegraven & Krusat 1991; Kielan-Jaworowska *et al.* 2004; Martin 2018).

At least 14 docodontan genera are known from dentomandibular remains from across Laurasia, and spanning in time the Middle Jurassic (Waldman & Savage 1972; Kermack *et al.* 1987; Sigogneau-Russell 2003) to the Early Cretaceous (Maschenko *et al.* 2002; Sigogneau-Russell 2003; Averianov *et al.* 2018), with a peak in taxonomic diversity in the Middle to Late Jurassic (Luo & Martin 2007; Panciroli *et al.* 2021a). One of the geologically oldest docodontans is *Borealestes*, a genus first discovered in the Kilmaluag Formation in Scotland, which is Bathonian in age, *c.* 166 Ma (Waldman & Savage 1972; Panciroli *et al.* 2021a). It was originally known only from dentomandibular remains referred to the type species *B. serendipitus* (Waldman & Savage 1972), with a more complete skeleton first discovered in 1972, but not studied until recently (Panciroli *et al.* 2018, 2019, 2021a). The partial skeleton of a second species, *Borealestes cuillinensis*, was identified from the same locality in 2018, and its crania described alongside those of *B. serendipitus* (Panciroli *et al.* 2021a).

The specimens of two species of *Borealestes* currently comprise the most complete skeletons for any Mesozoic mammaliaform in the UK. *Borealestes* has long been considered part of a basal docodontan clade, based on phylogenetic analyses using dentomandibular characters (Sigogneau-Russell 2003; Martin & Averianov 2004; Luo & Martin 2007; Averianov *et al.* 2010; Panciroli *et al.* 2019, 2021a). As one of the geologically oldest docodontan genera it provides critical information on the emergence of this clade; their morphology is of particular interest for reconstructing the ecology and early evolution of Docodonta. Herein we describe the postcrania of *Borealestes serendipitus* and *B. cuillinensis*, and address their phylogenetic placement in a more comprehensive dataset including characters from across the skeleton. We analyse the postcrania of *Borealestes* for ecological signatures using comparative morphology, with the addition of 3D geometric morphometrics. This will allow us to maximize the

information gained from the girdle and limb bones, which are exceptional in being preserved with minimal deformation or compression, making them especially informative for assessment of the morphology of this taxon, with implications for early mammal evolution.

## MATERIAL AND METHOD

### *Specimens*

NMS G.1992.47.121.1 is the partial skeleton of *B. serendipitus* (Fig. 1), discovered in 1972 during fieldwork led by R. Savage and M. Waldman on the shoreline south of Cladach a'Ghlinne, Isle of Skye (Fig. 2A). It was collected in 1973 and mechanically prepared by S. Finney at the University of Cambridge between 1994 and 1996, using a sodium bicarbonate airbrasive. It was then consolidated with 2% Paraloid B72. Some portions of the skeleton are detached from the limestone block (it is unclear when this occurred) and are stored separately (see Table 1 for full details). Only the postcranial elements are described herein; a full description of the crania and dentition are already provided elsewhere (Panciroli *et al.* 2021a).

NMS G.2020.4.1.1 is the partial skeleton of the recently named species *B. cuillinensis* (Panciroli *et al.* 2021a), found at Cladach a'Ghlinne in 2018 by Prof. Richard Butler during fieldwork by the University of Oxford, National Museums Scotland and University of Birmingham (Fig. 2B). It was removed in the field using a rock saw, and reduced in size by brittle fracture, without loss of material. We used using an iterative process of pilot x-ray micro-computed tomography ( $\mu$ CT) scanning to facilitate minimum-loss block-splitting and removal of excess matrix using lab-based rock cutting equipment (carried out by RBB) resulting in a specimen composed of several separate, but contiguous blocks that could each be scanned at high resolution (see Fig. 2B and Table 1). Only the postcranial elements are described herein (see Panciroli *et al.* 2021a for full description of the crania and dentition).

### *X-ray micro-computed tomography and data processing*

The parameters used for each acquisition of  $\mu$ CT are listed in Table 1. NMS G.1992.47.121.1 was scanned at the European Synchrotron Radiation Facility (ESRF, Grenoble, France) using propagation phase contrast  $\mu$ CT. It was scanned at a lower resolution to capture the whole skeleton, and at higher resolution in the area containing the skull. Although the skull was described by Panciroli *et al.* (2021a), some of the postcranial bones in the area of the skull are newly described herein (Fig. 1).

X-ray  $\mu$ CT data for NMS G.1992.47.121.2, NMS G.1992.47.121.4, NMS G.1992.47.121.5, NMS G.1992.47.121.6, NMS G.1992.47.121.7, NMS G.1992.47.121.8, NMS G.1992.47.121.9, NMS G.1992.47.121.10, NMS G.1992.47.121.11, and NMS G.1992.47.121.12 were obtained at the University of Edinburgh by Dr I. Butler, School of Geosciences Experimental Geoscience Facility, using their in-house built  $\mu$ CT scanner. The system comprises a Feinfocus 10–160 kV dual transmission/reflection source (Feinfocus Röntgen-Systeme GmbH, Garbsen, Germany), MICOS UPR-160-AIR ultra-high precision air-bearing table (PI miCos GmbH, Eschbach, Germany), Perkin Elmer XRD0822 amorphous silicon x-ray flat panel detector and terbium doped gadolinium oxy-sulfide scintillator (PerkinElmer, Waltham, MA, USA). Data acquisition software was written in-house, and tomographic reconstruction were performed by I. Butler using Octopus 8.7 software (TESCAN Orsay Holding a.s., Brno, Czech Republic).

X-ray  $\mu$ CT data for NMS G.1992.47.121.3 and NMS G.2020.4.1.1 were obtained by RBB and Dr T. Davies at the University of Bristol using a Nikon XTH 225 ST (Nikon Metrology, Leuven, Belgium) with a 225 kV rotating target.

All tomographic data were segmented and digitally reconstructed by EP using Mimics 19.0 (Materialise NV, Leuven, Belgium) at NMS and the University of Oxford. Where fossils were not covered completely by sedimentary matrix, they were also examined using conventional light microscopy at NMS. Measurements were taken using the measurement tools in Mimics 19.0, and corroborated with manual measurements using fine callipers or a microscope where possible.

### *Phylogenetic analysis*

To assess the phylogenetic placement of *Borealestes* species within Docodonta in light of newly available cranial and postcranial characters, we used the matrix of Zhou *et al.* (2019), adding scores for *B. serendipitus* and *B. cuillinensis*. This dataset includes 128 taxa scored for 556 characters: 40 mandibular; 187 dental; 145 postcranial; 176 cranial characters and 8 soft-tissue characters. *Borealestes serendipitus* was scored for 278 characters (50%) and *B. cuillinensis* for 250 characters (45%), which is comparable with the other docodontans in this matrix such as *Castorocauda* (42%), *Docofossor* (45%), and *Microdocodon* (52%), but less complete than *Haldanodon* (63%) or *Agilodocodon* (63%).

Parsimony analyses were carried out using most of the same search parameters as Zhou *et al.* (2019), using PAUP v.4 (Swofford 2003). As for Zhou *et al.*, an heuristic search was carried out with characters equally weighted, and unordered, the branch swapping algorithm was tree



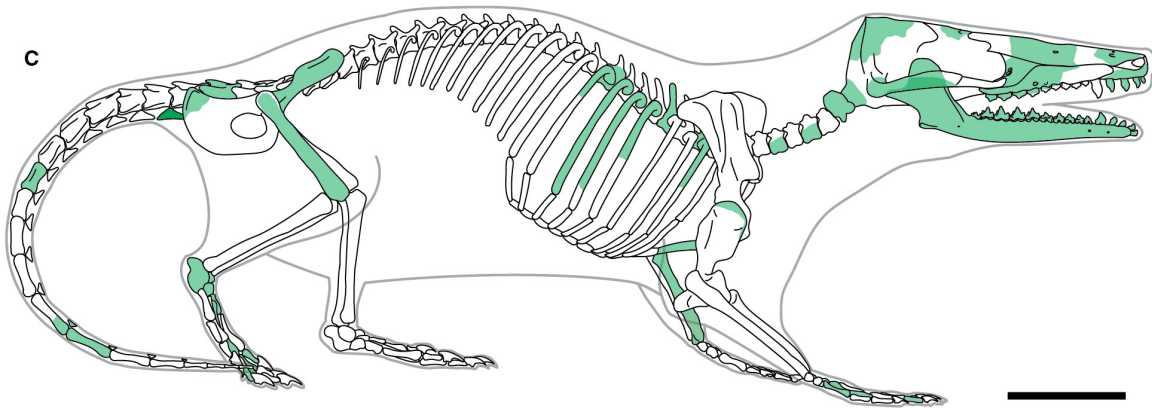
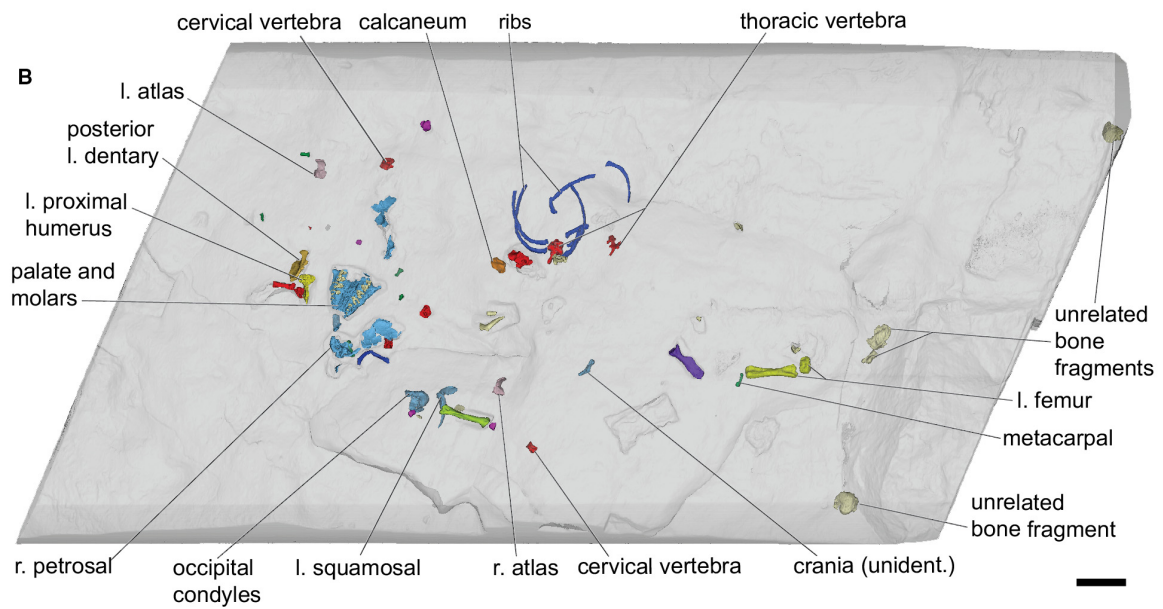
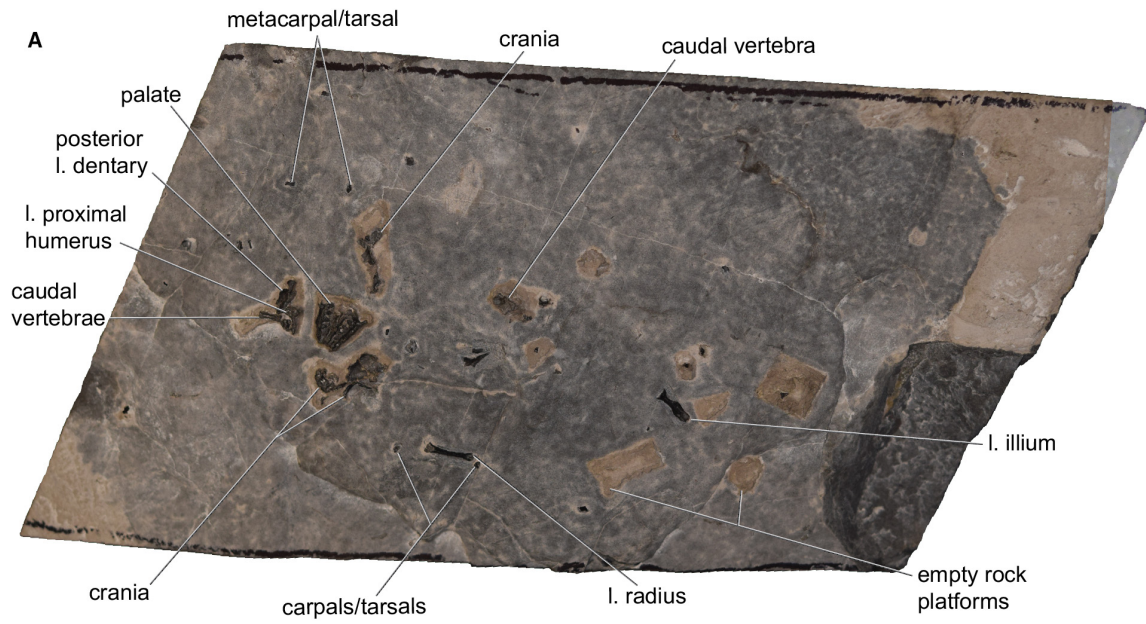


**FIG. 1.** *Borealestes serendipitus* NMS G.1992.47.121.1. A, photograph of NMS G.1992.47.121.1. B, from synchrotron CT data with matrix semi-transparent, showing skeletal elements within the block. C, reconstruction of *B. serendipitus*' skeleton, with bones present in NMS G.1992.47.121.1 highlighted in green. Details of skull elements in Panciroli *et al.* (2021a); l, left; r, right. Scale bars represent 10 mm.

bisection reconnection (TBR), with a reconnection limit of 8 and steepest descent option in effect. Our analysis differs from that of Zhou *et al.* in that trees were obtained using stepwise addition with one tree held at each step and the addition sequence random, with 5000 replicates whereas Zhou *et al.* used 10 000 replicates, and MulTrees was turned on, because turning it off reduces the ability of branch-swapping to find the best tree.

We carried out four analyses: (1) Zhou *et al.*'s (2019) original matrix (which did not include *Borealestes*); (2) the original matrix without *Borealestes*, but amending character scores for characters 32, 56, 67, 127, 131, 133, 312, 362 and 522 for docodontans, where our interpretation differed from that of the previous authors' (see Panciroli *et al.* 2021b); (3) Zhou *et al.*'s (2019) original matrix with *Borealestes* species added; (4) as for analysis 2, adding *Borealestes* species. We used PAUP statistical tools to obtain the consistency index (CI), homoplasy index (HI), retention index (RI) and rescaled consistency index (RC) for all analyses (Table 2). See Panciroli *et al.* (2021b) for more details.

#### Geometric morphometric analysis

The postcrania of *Borealestes* species were analysed using principal components analysis (PCA) on 3D landmarks, to compare their shape with extant taxa and provide additional data to make inferences for locomotor and ecological specializations. This approach was not intended to provide an exhaustive analysis, but to augment our comparative analysis and maximize the information gained from the preserved elements. Due to being incomplete, 2D linear measurements and indices of all major limbs (e.g. Chen & Wilson 2015; Meng *et al.* 2017) cannot easily be implemented, but the limited number of limb bones being preserved with minimal compression/distortion can easily be incorporated into 3D analyses. Using single elements of the limb to infer locomotor function can be successful (e.g. Kilbourne 2017; Janis & Martín-Serra 2020), however relying on single elements can also be uninformative when ecomorphological variation is not adequately captured by such landmark constellations. The 2D landmark analysis of bones such as the humerus and ulna has also proven informative for examining ecomorphology and evolution of pre-mammaliaform therapsids (e.g. Lungmus & Angielczyk 2019).

We applied the 3D landmark and semilandmark scheme of Martín-Serra & Benson (2020) to the radius, pelvis

(only the ilium) and femur of *B. serendipitus*, and the ulna, humerus and scapulacoracoid of *B. cuillinensis*, because these were the most complete postcranial elements. We analysed these in the context of a dataset of 42 extant mammals held in multiple collections (Table 3). Extant species were selected to include members from different groups of Marsupialia and Placentalia in each ecological/locomotor category, also including the platypus, *Ornithorhynchus anatinus*, as a representative of Monotremata. Based on the mandibular lengths (Table 4), we estimate a body mass of up to 40 g for *B. serendipitus*, and 16 g for *B. cuillinensis* (Foster 2009; Panciroli *et al.* 2021b), this is similar to extant mammals such as *Oryzoryctes* (tenrec) and *Neomys* (shrew) respectively (Table 3). Therefore we have predominantly selected extant taxa weighing <1 kg (30 out of 42), to minimize the over-representation effect of taxa with larger body mass on the ecomorphological signature, as in previous comparative studies of the locomotor ecomorphology of Mesozoic mammals (e.g. Chen & Wilson 2015; Meng *et al.* 2017; Grossnickle *et al.* 2020). We assigned the therian taxa to five categories based on their ecology and locomotion: scratch diggers, swimmers, arboreal, runners (cursorial), gliders and 'generalists' (Table 3). The term 'generalist', widely used in previous literature, is employed in this study as a category for predominantly terrestrial mammals that, although capable of some of the ecological behaviours identified for other taxa, lack highly derived ecological or locomotor specializations or their associated morphologies (Polly 2007). Our use of the term 'generalist' is not intended to imply that these taxa are incapable of performing diverse ecological behaviours. Indeed, many of these taxa may be capable of climbing, scratch digging and other behaviours (e.g. *Apodemus sylvaticus* or *Myrmecobius fasciatus*) but nevertheless lack the morphological features of more specialized taxa. This may be widespread in small bodied taxa in which ecomorphological signatures may generally be less pronounced (Weaver & Grossnickle 2020). This decision does not impede our primary aim of identifying ecomorphological specializations in extinct species.

Extant mammals were CT-scanned, digitally segmented, and 3D landmarks and semilandmarks placed using Avizo (FEI Visualization Sciences Group 2015; Panciroli & Benson 2021). Our landmarks and semilandmarks (see Martín-Serra & Benson 2020) were selected to capture traits of the bones such as overall shape and tuberosities that mark the positions of muscle attachments, or edges of articular surfaces. Because of damage and incompleteness,

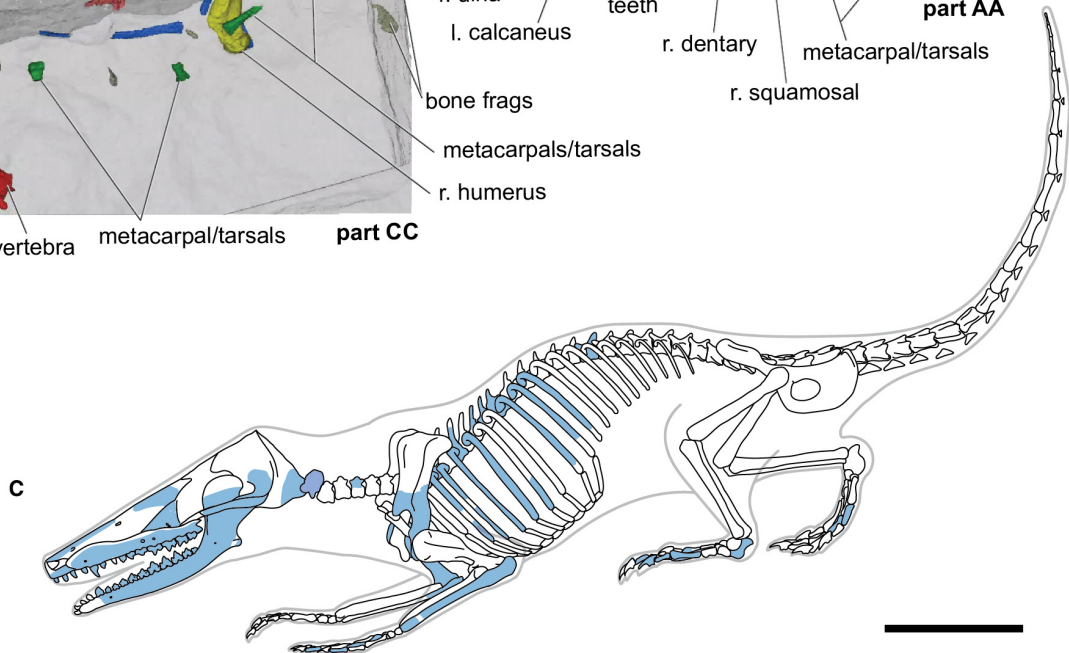
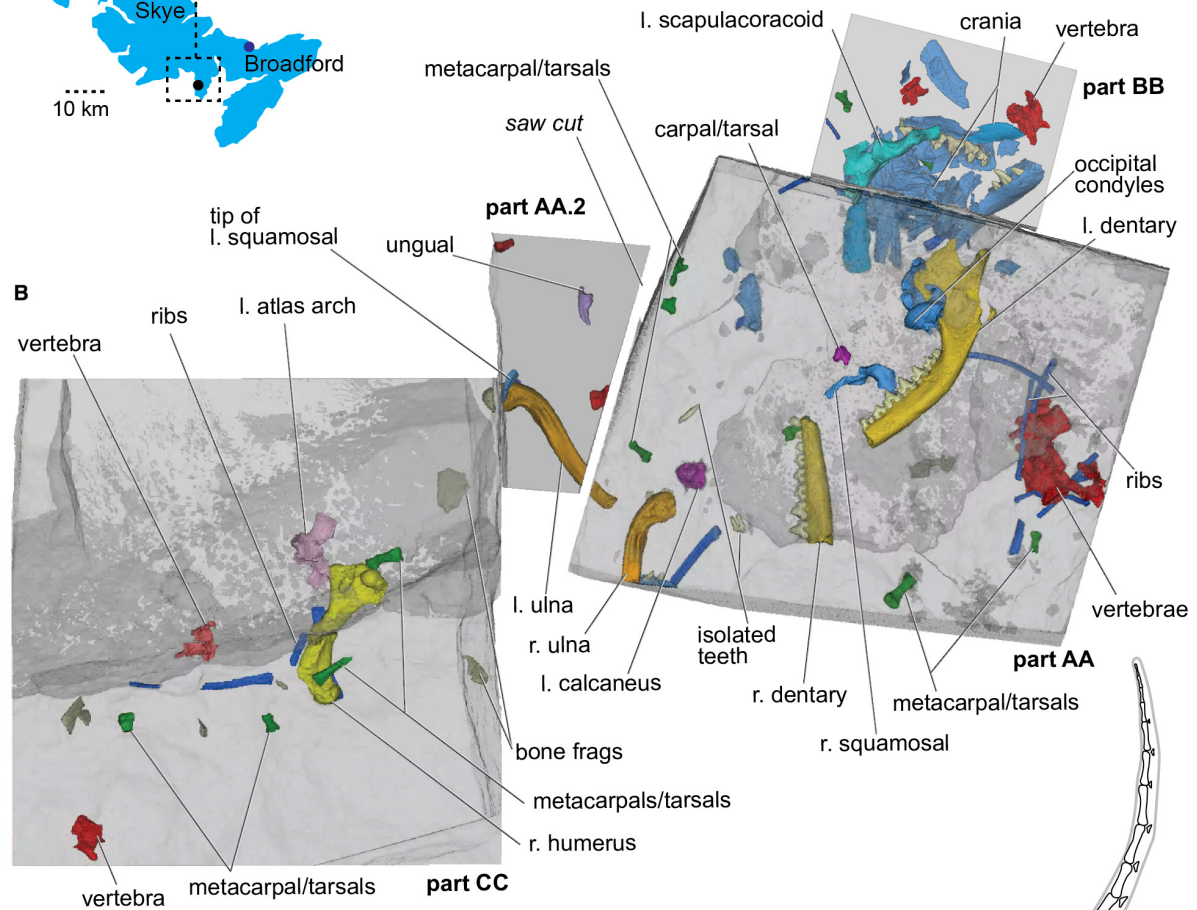
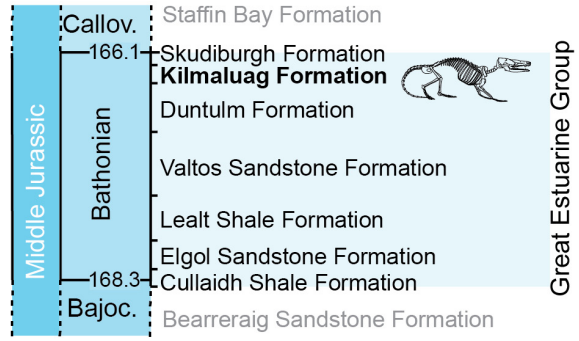
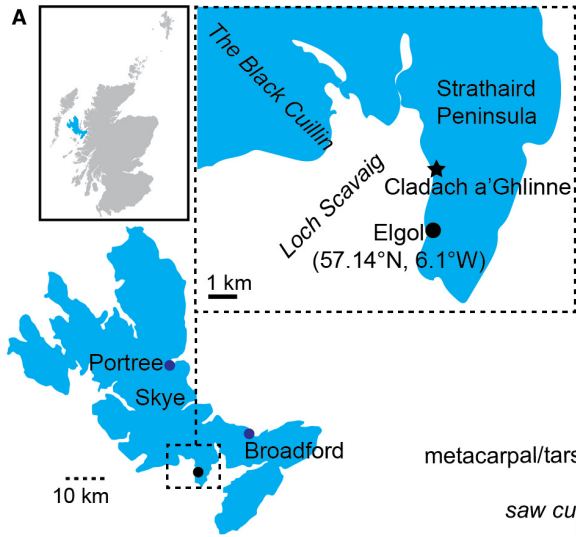


**FIG. 2.** Locality of specimens, and *Borealestes cuillinensis* NMS G.2020.4.1.1. A, location of the *Borealestes* specimen site on the Isle of Skye, and the geological context. B, NMS G.2020.4.1.1 (with separate parts labelled; see Material and Method and Table 1 for details) from  $\mu$ CT data with matrix semi-transparent, showing skeletal elements within the blocks. C, reconstruction of *B. cuillinensis*' skeleton, with bones present in NMS G.1992.47.121.1 highlighted in blue. Scale bar represents 10 mm (B, C).

not all landmarks could be placed on the *Borealestes* specimens, but a total of 19 landmarks and 12 semilandmark series were identifiable across all elements (Table 5; Fig. 3). Only those landmarks preserved on the *Borealestes* specimens were used from the extant taxa in our analyses, so our analyses effectively include: (1) scapula, the glenoid facet, position of acromion and curve of the scapular neck; (2) humerus, shape of the proximal and distal articular surfaces, shape of the pectoral/deltoid crests and tuberosities, width of the distal humerus; (3) ulna, shape of the proximal articular surface, length and shape of the olecranon process, length of the proximal portion of the ulna vs the distal, overall length of the ulna; (4) radius, shape of the proximal articular surface and its proximal extent; (5) femur, shape of the distal articulation; (6) pelvis, length and shape of the dorsal edge of the ilium. For full details of the 3D landmarking scheme see Panciroli *et al.* (2021b).

We used R v.3.4.1 (R Core Team 2017) and functions from the R package geomorph (Adams *et al.* 2017) to analyse morphometric data. We performed a generalized Procrustes superimposition on the three-dimensional coordinates of the landmarks and semilandmarks (Dryden & Mardia 1998) to remove the effects of size, translation, orientation, and the spacing of sliding semilandmarks. We then used the plotTangentSpace function of geomorph (Adams *et al.* 2017) to perform the PCA on the Procrustes (shape) coordinates. This provides the consensus (mean) shape and three-dimensional coordinates of the extreme shapes of each PC which were visualized using geomorph functions mshape, warpRefMesh and plotRefToTarget (Adams *et al.* 2017), generating three-dimensional surfaces that represent the theoretical shape changes along PC axes. Plots were then finalized in Adobe Illustrator v.20 (Adobe Inc.)

*Institutional abbreviation.* NMS (formerly RSM), National Museums Scotland, Chambers Street, Edinburgh, UK.

## RESULTS

### Phylogenetic analysis

The shortest-length trees recovered from each of the four phylogenetic analyses are shown in Figure 4C–F, focusing on relationships within Docodontia (full details can be found in Panciroli *et al.* 2021b). All four analyses returned a similar topology for the docodontan clade,

with *Agilodocodon* and *Microdocodon* as sister-taxa, and *Borealestes* species as sister taxa to *Agilodocodon* + *Microdocodon*, but the placement of *Haldanodon*, *Castorocauda* and *Docofossor* is variable among permutations of analyses.

*Analyses 1 and 2.* We re-analysed the Zhou *et al.* (2019) matrix with modified search parameters (see Material and Method, above) and returned one tree of 2826 steps (Zhou *et al.* 2019 recovered a single tree of 2808 steps). *Castorocauda* and *Docofossor* are found in a different arrangement than Zhou *et al.* (Fig. 4A, C), but *Haldanodon* remains in a similar position, although it is a sister taxon to *Castorocauda* in this analysis. *Agilodocodon* and *Microdocodon* are sister-taxa as in Zhou *et al.* Analysis 2, in which we modified the character scores for docodontan taxa, returned a single tree of 2835 steps with the same tree topology as the original analysis by Zhou *et al.* (Fig. 4A, D)

*Analyses 3 and 4.* We added *B. serendipitus* and *B. cuillinensis* to the original Zhou *et al.* (2019) matrix (Analysis 3), and with updated characters for docodontans (Analysis 4), returned single trees of 2850 (Analysis 3) and 2841 (Analysis 4) steps (Fig. 4E, F). There is little effect on the overall topology of the docodontan tree: *Haldanodon*, *Castorocauda* and *Docofossor* remain as earlier-branching taxa, whereas *Borealestes* species are sister-taxa, closely related to the sister-taxa *Agilodocodon* and *Microdocodon*.

Dental and cranial character states identified in Analysis 4 as uniting the *Borealestes* species include: a less developed Meckel's sulcus than other docodontans (Char. 5(1)); the presence of a pterygoid fossa on the medial side of the ramus of the mandible (Char. 19(1)); presence of a shelf for the pterygoid on the ventral border of the mandible (Char. 20(1)); the presence of a mandibular foramen inside the masseteric fossa (Char. 24(1)); the presence of a diastema posterior to the PM1 (Char. 52(1)); the presence of a cuspule in addition to cusp c in the ultimate lower premolar (Char. 58(2)); the absence of crenulation or cuspules on cingulid row of the lower premolars (Char. 63(0)); the absence of an a-g crest (Char. 99(0)); the interlocking of the molars (Char. 102(1)); the relatively small upper canine (Char. 185(1)); lack of procumbency in the PM1 (Char. 197(0)). Postcranial characters uniting the *Borealestes* species include: the expanded and helical articular surface of the clavicle (Char. 248(1)); the short, dorso-ventrally compressed calcaneal tuber without

**TABLE 1.** List of parameters used for  $\mu$ CT acquisition of the specimens.

Specimen number and part	Element	Publication	CT system	Voxel size ( $\mu$ m)	No. of proj.	Filter (mm)	kV	$\mu$ A	Power (W)	Exp. (s)	Fr. av.
NMS G.2020.4.1.1, Part AA	Part of whole skeleton <i>B. cuillimensis</i>	Herein & Panciroli <i>et al.</i> 2021a	Nikon XTH 225 ST (UoB)	22.14	2201	Cu 0.5	180	111	19.98	0.708	4
NMS G.2020.4.1.1, Part AA.2	Part of whole skeleton <i>B. cuillimensis</i>	Herein	Nikon XTH 225 ST (UoB)	20.05	3141	None	130	154	20.02	0.5	4
NMS G.2020.4.1.1, Part BB	Part of whole skeleton <i>B. cuillimensis</i>	Herein & Panciroli <i>et al.</i> 2021a	Nikon XTH 225 ST (UoB)	20.05	3141	None	130	154	20.02	0.5	4
NMS G.2020.4.1.1, Part CC	Part of whole skeleton <i>B. cuillimensis</i>	Herein	Nikon XTH 225 ST (UoB)	29.40	3141	Cu 0.5	221	131		1.415	4
NMS G.1992.47.121.1	Whole skeleton <i>B. serendipitus</i>	Herein	ESRF	11.90	6000	Al 5.6 Cu 10				11.90	6000
NMS G.1992.47.121.1	Whole skeleton <i>B. serendipitus</i> (section around skull)	Herein & Panciroli <i>et al.</i> 2021a	ESRF	6.15	6000	Al 5.6 Cu 5.6 W 0.5	201			0.3	
NMS G.1992.47.121.2	Left petrosal	Panciroli <i>et al.</i> 2018	In-house built $\mu$ CT (UoE)	8.9	2000	Al 0.8	70	40	2.8	2	n.a
NMS G.1992.47.121.3	Right dentary	Panciroli <i>et al.</i> 2019	Nikon XTH 225 ST (UoB)	12.77	*	*	*	*	*	*	*
NMS G.1992.47.121.4	Premaxilla & nasal fragment	Panciroli <i>et al.</i> 2021a	In-house built $\mu$ CT (UoE)	6.43	*	None	*	*	*	*	*
NMS G.1992.47.121.5	Metatarsal (mt3)	Herein	In-house built $\mu$ CT (UoE)	8.9	2000	Al 0.8	70	40	2.8	2	n.a
NMS G.1992.47.121.6	Right clavicle	Herein	In-house built $\mu$ CT (UoE)	8.9	2000	Al 0.8	70	40	2.8	2	n.a
NMS G.1992.47.121.7	Carpal/tarsal element	Herein	In-house built $\mu$ CT (UoE)	8.9	2000	Al 0.8	70	40	2.8	2	n.a
NMS G.1992.47.121.8	Chevron	Herein	In-house built $\mu$ CT (UoE)	8.9	2000	Al 0.8	70	40	2.8	2	n.a
NMS G.1992.47.121.9	?Cranial fragment	Herein	In-house built $\mu$ CT (UoE)	8.9	2000	Al 0.8	70	40	2.8	2	n.a
NMS G.1992.47.121.10	CARPAL/tarsal element	Herein	In-house built $\mu$ CT (UoE)	8.9	2000	Al 0.8	70	40	2.8	2	n.a
NMS G.1992.47.121.11	Fragment of ischium	Herein	In-house built $\mu$ CT (UoE)	8.9	2000	Al 0.8	70	40	2.8	2	n.a
NMS G.1992.47.121.12	Fragment of rib	Herein	In-house built $\mu$ CT (UoE)	8.9	2000	Al 0.8	70	40	2.8	2	n.a

Exp., exposure time; fr. av., frame averaging; No. of proj, number of projections.

ESRF, European Synchrotron Radiation Facility; UoB, University of Bristol; UoE, University of Edinburgh.

For ESRF parameters, the voltage column (kV) indicates the detected total integrated energy in keV.

\*Missing data.



**TABLE 2.** Results of statistical analyses on phylogenetic analyses.

Analysis	Tree length	CI	HI	RI	RC
1	2826	0.3181	0.6819	0.7968	0.2535
2	2850	0.3154	0.6850	0.7988	0.2520
3	2835	0.3171	0.6829	0.7959	0.2524
4	2841	0.3164	0.6836	0.7998	0.2531

CI, consistency index; HI, homoplasy index; RI, retention index; RC, rescaled consistency index.

a terminal swelling (Char. 319(0)); the absence of a saddle-shaped contact between entocuneiform and proximal end of metatarsal 1 (Char. 341(1)); the presence of an external auditory meatus on the zygoma (Char. 362(0)); and the presence of a stapedial artery sulcus on the petrosal (Char. 414(1)). Several of these characters are not preserved in *B. cuillinensis*, and are scored as ?, but are inferred as present in *B. cuillinensis* by our Analysis 4, and returned as character states for the node that unites them as sister-taxa.

#### Geometric morphometrics

The results for PC1, PC2 and PC3 are given in Table 6 (for fully labelled PCA results see Supporting Information or Panciroli *et al.* 2021b). Across all analyses  $\geq 59\%$  of the variation is explained by the first two PC axes, and  $\geq 70\%$  of the variation is explained by the first three PC axes (Figs 5, 6). *Borealestes* mostly falls in or near the morphospace occupied by extant therians on PC1 and PC2, and most often within that occupied by taxa with unspecialized morphology (so-called ‘generalists’) but is separated from all taxa in analysis of the femur, and most extant taxa on PC3 in analyses of the scapula, humerus (along with *Ornithorhynchus*) and ulna (Fig. 6A–C). PC3 in these analyses may therefore describe the difference between extant therians and *Borealestes* as a stem-group mammal outside the extant radiation (crown/stem terminology used herein *sensu* Budd & Jensen 2000).

*Borealestes* and *Ornithorhynchus* occupy a similar position on the positive PC1 of the PCA of the radius (Fig. 5A), but other extant taxa plot nearby, so the similarity of *Borealestes* and *Ornithorhynchus* in this regard is not unique; unlike the similarity of their humeri (see below). Only one landmark and one semilandmark series are included for the radius (Fig. 3D), and positive scores on PC1 reflect a rounder proximal articulation, whereas negative scores reflect a more oblong proximal articulation. Scores for PC2 and PC3 capture very slight elongation in the shape of the proximal articulation relative to the proximal tip of coronoid process (landmark L1,

Fig. 3D) in PC2. This effectively separates the arboreal (and gliding) taxa, from the scratch diggers and swimmers, with *Borealestes* scoring similarly to the latter two groups.

In the PCA of the pelvis, *Borealestes* falls near extant taxa on all three axes (Fig. 5B). Our analysis for this bone only captures the medial and dorsal edge of the ilium (Fig. 3F). PC1 scores reflect changes in the dorsal edge of the ilium, being either convex dorsally (positive scores) or concave (negative scores). PC2 reflects the position of the intersection of the ventral and anterior edge of iliac crest, which flares laterally relative to the rest of the anterior edge of the crest in taxa that score positively on this axis. PC3 reflects the shape of the anterior edge of the iliac crest: a more anteriorly expanded crest in taxa scoring negatively, and a reduction or virtual absence of the anterior edge of the crest in those scoring positively.

The PCA of the femur (which only incorporates the distal articulation because the proximal part is not complete in these fossils, see Fig. 3E) places *Borealestes* in a completely separate area of morphospace to that of all extant mammals in our dataset (Fig. 5C). *Borealestes* and *Ornithorhynchus* score negatively on PC1, which captures their wider mediolateral width of the distal articulation. However, *Ornithorhynchus* scores similarly on PC2 to extant therian mammals, whereas *Borealestes* scores more positively, reflecting the comparatively large anteroventral articulating surface of the distal femur. Although scoring more similarly to extant therians than *Borealestes*, *Ornithorhynchus* falls outside of their morphospace, scoring more negatively on PC1 and PC3.

*Borealestes* and *Tarsipes* have a negative score on PC3 in the analysis of the scapula (Fig. 6A). Our analysis is essentially confined to the shape of the glenoid facet, curvature of the edge of the scapular neck, and position of the acromion (Fig. 3A). Negative scores on PC3 reflect a dorsoventrally elongate glenoid facet (rather than round), a more dorsally located acromion, positioned at mid-height relative to the glenoid facet, and the point of maximum curvature of the anterior edge of the scapular neck ventral relative to the posterior edge of the scapular neck (Fig. 6A). *Ornithorhynchus* plots at the extreme negative PC2 and positive PC3 in this analysis, completely separating it from both the extant therians, and *Borealestes*.

*Borealestes* and *Ornithorhynchus* occupy somewhat similar positions in morphospace on PC3 of the PCA on the humerus (Fig. 6B), where they both fall well outside the area occupied by other extant taxa. *Borealestes* falls at an intermediate location between the well-defined cluster for therian mammals (with positive PC3 scores), and the position occupied by *Ornithorhynchus* (with negative PC3 scores). The humerus is one of the two most completely landmarked bones in our analysis (along with the ulna, each incorporating almost all the landmarks from Martín-

**TABLE 3.** Extant taxa used in principal components analyses, arranged by body mass.

Taxon	Specimen number	Common name	Order	Family	BM (g)	E/L
<i>Acrobates pygmaeus</i>	NHMUK 82.7.29.23–24	Feathertail glider	Diprotodontia	Acrobatidae	12	GL
<i>Amblysomus hottentotus</i>	UMZC 2010.15a	Hottentot golden mole	Afrosoricida	Chrysochloridae	53	FD
<i>Antechinomys laniger</i>	NHMUK 32.2.11.23	Kultarr	Dasyuromorphia	Dasyuridae	27	R
<i>Apodemus sylvaticus</i>	NHMUK unnumbered	Wood mouse	Rodentia	Muridae	22	G
<i>Caluromysiops irrupta</i>	FMNH 60698	Black-shouldered opossum	Didelphimorphia	Didelphidae	250	A
<i>Castor canadensis</i>	AMNH 150136	North American beaver	Rodentia	Castoridae	21820	S
<i>Dromicia concinna</i>	NHMUK 1897.11.18.1	Western pygmy possum	Diprotodontia	Burrmyidae	13	A
<i>Dactylopsila trivirgata</i>	NHMUK 1897.8.7.79	Striped possum	Diprotodontia	Petauridae	404	A
<i>Dasyprocta punctata</i>	FMNH 60569	Central American agouti	Rodentia	Dasyproctidae	2675	R
<i>Dendrohyrax arboreus</i>	FMNH 163770	Southern tree hyrax	Hyracoidea	Procaviidae	2950	A
<i>Dendrolagus dorianus</i>	NMS 2006.38	Doria's tree-kangaroo	Diprotodontia	Macropodidae	9581	A
<i>Desmana moschata</i>	UMMZ 124125	Russian desman	Eulipotyphla	Talpidae	383	S
<i>Didelphis marsupialis</i>	NHMUK 1948.7.12.5	Common opossum	Didelphimorphia	Didelphidae	1091	A
<i>Diplomesodon pulchellum</i>	FMNH 137436	Piebald shrew	Eulipotyphla	Soricidae	11	G
<i>Elephantulus rozeti</i>	NHMUK 1891.10.15.11	North African elephant shrew	Macroscelidea	Macroscelididae	48	R
<i>Enhydra lutris</i>	NHMUK 80.879	Sea otter	Carnivora	Mustelidae	23500	S
<i>Euroscaptor micrura</i>	NHMUK 99.10.25.1	Himalayan mole	Eulipotyphla	Talpidae	60	FD
<i>Glis glis</i>	NHMUK 1996.325	Edible dormouse	Rodentia	Gliridae	125	A
<i>Hemiechinus auritus</i>	UMMZ 156626	Long-eared hedgehog	Eulipotyphla	Erinaceidae	342	G
<i>Idiurus zenkeri</i>	UMZC E.1421	Pygmy scaly-tailed flying squirrel	Rodentia	Anomaluridae	100	GL
<i>Leopardus wiedii</i>	NMS 2016.12.1	Margay	Carnivora	Felidae	3250	A
<i>Limnogale mergulus</i>	FMNH 165440	Web-footed tenrec	Afrosoricida	Tenrecidae	80	S
<i>Lutreolina crassicaudata</i>	UMMZ 134562	Lutrine opossum	Didelphimorphia	Didelphidae	537	S
<i>Macroscelides proboscideus</i>	FMNH 137045	Round-eared elephant shrew	Macroscelidea	Macroscelididae	38	R
<i>Macrotis lagotis</i>	NHMUK 73.6.21.4	Greater bilby	Peramelemorphia	Peramelidae	1350	R
<i>Microgale thomasi</i>	UMMZ 172202	Thomas's shrew tenrec	Afrosoricida	Tenrecidae	23	G
<i>Myosorex kahaulei</i>	FMNH 209072–209073	Kihaule's mouse shrew	Eulipotyphla	Soricidae	10	G
<i>Myrmecobius fasciatus</i>	UMZC A6.41/8	Numbat	Dasyuromorphia	Myrmecobiidae	472	G
<i>Nandinia binotata</i>	UMZC K.4492	African palm civet	Carnivora	Nandiniidae	2000	A
<i>Neomys fodiens</i>	NHMUK 1973.917	Eurasian water shrew	Eulipotyphla	Soricidae	14	S
<i>Notoryctes typhlops</i>	UMZC A5.1/1	Southern marsupial mole	Notoryctemorphia	Notoryctidae	55	FD
<i>Ornithorhynchus anatinus</i>	UMZC A2.2/10	Platypus	Monotremata	Ornithorhynchidae	2000	S
<i>Oryctolagus cuniculus</i>	NHMUK 1849.6.20.9	European rabbit	Lagomorpha	Leporidae	1767	R
<i>Oryzicetes tetradactylus</i>	UMZC E.5453c	Four-toed rice tenrec	Afrosoricida	Tenrecidae	36	FD
<i>Petaurus breviceps</i>	FMNH 129430	Sugar glider	Diprotodontia	Petauridae	106	GL
<i>Petinomys sagitta</i>	UMZC E.1499	Arrow flying squirrel	Rodentia	Sciuridae	50	GL
<i>Procavia capensis</i>	FMNH 147999	Rock hyrax	Hyracoidea	Procaviidae	3030	G
<i>Solenodon paradoxus</i>	FMNH 51068	Solenodon	Eulipotyphla	Solenodontidae	900	G
<i>Sylvisorex howelli</i>	FMNH 198206	Howell's forest shrew	Eulipotyphla	Soricidae	4	G
<i>Tarsipes rostratus</i>	UMMZ 122547	Honey possum	Diprotodontia	Tarsipidae	9	A
<i>Trichosurus vulpecula</i>	UMZC A9.16/7	Common brushtail possum	Diprotodontia	Phalangeridae	2650	A
<i>Tupaia glis</i>	UMZC E.4057E	Common Treeshrew	Scandentia	Tupaiaidae	170	A

BM, body mass; E/L, ecological/locomotor categories: A, arboreal; FD, forelimb digger; G, generalist; GL, glider; R, runner; S, swimmer.

AMNH, American Museum of Natural History, New York, USA; FMNH, Field Museum of Natural History, Chicago, USA; UMMZ, University of Michigan Museum of Zoology, USA; NHMUK, Natural History Museum, London, UK; NMS, National Museums Scotland, Edinburgh, UK; UMZC, University Museum of Zoology, Cambridge, UK.

Body mass data from Geiser (1986), Nowak (1999), Smith *et al.* (2003).

**TABLE 4.** Measurements of dentary and select elements of the appendicular skeletons of *Borealestes*.

Taxon	Specimen number	Dentary	Humerus	Radius	Ulna	Femur	Ilium
<i>Borealestes serendipitus</i>	NMS G.1992.47.121.1 & NMS G.1992.47.121.3	23.3	–	12.3	–	12.82*	9.8
<i>Borealestes cuillinensis</i>	NMS G.2020.4.1.1	17.3	10.396*	–	11.2*	–	–

Measurements in mm.

\*Estimate (where bone is broken/part missing).

Serra & Benson 2020) (Fig. 3B; Table 5). Negative scores on PC3 reflect a narrower radial and ulnar condyle in *Borealestes* and *Ornithorhynchus*, and a larger, flared deltopectoral crest without clear distinction between the edges of the deltoid and pectoral crests (captured by SL2 and SL3). The proximal articular surface of the humerus is also much larger. PC1 in the PCA of the humerus effectively separates the specialist digging taxa from the rest of the dataset. These taxa score negatively on this axis, reflecting a much sturdier, wider humerus along the length of the bone, but particularly distally, a much larger distal articulation, and flared deltopectoral crest (Fig. 6B). Meanwhile PC2 captures the position of the most medial point of the medial epicondyle (entepicondyle), the position of the proximal origin of the lateral epicondylar crest, the amount of elongation in the proximal portion of the humerus, and the relative position of the humeral head (displaced laterally in taxa scoring negatively on this axis).

In the analysis of the ulna, *Borealestes* scores negatively on PC3, as do *Enhydra* and *Euroscaptor* (Fig. 6C). Along with the humerus, the ulna is one of the two most completely landmarked bones in our analysis (Fig. 3C). Negative scores on PC3 reflect a relatively straight medial edge of the olecranon process, the ulna being mediolaterally wide medial to the articular surface of the olecranon, and the distal portion of the olecranon itself being dorsoventrally wide, with a dorsoventrally elongate articular surface of the olecranon. PC1 in the analysis of the ulna captures the overall length of the ulna, and the relative length of the proximal versus distal portions of the ulna. Negative scores on this axis reflect an elongate, wide olecranon process and relatively short distal ulna, as seen in digging taxa, which score negatively on this axis, separating most of them from the remainder of the dataset. PC2 reflects the extent of mediolateral flaring of the olecranon process, and the size of the proximal articulation of the ulna. Scoring negatively on PC2, *Ornithorhynchus* is separated from both the extant therians, and *Borealestes*.

## DESCRIPTION

NMS G.1992.47.121.1 is a block of blue–grey limestone measuring approximately 183 mm in length, 105 mm in width, and between 148 and 340 mm in thickness

(Fig. 1A). NMS G.1992.47.121.1 was substantially larger when collected (*c.* 240 mm in length, *c.* 170 mm in width and *c.* 50 mm in depth) and was reduced in size by curators at NMS when it became clear the block required trimming to obtain successful scans at high resolution for study. All offcuts were retained. The surface is undulating, with hairline cracks in the prepared upper surface, also visible in synchrotron scan data. Skeletal elements are scattered on the surface of the block, including the palate and elements of the skull, left ilium and left radius (Fig. 1A). Synchrotron scans revealed other parts of the skeleton within the block (Fig. 1B). The surface bones sit on ‘platforms’ of rock, the result of acid and mechanical preparation to remove the surrounding rock. At least seven such platforms no longer contain fossil material, and probably indicate the original positions of bones that have been removed or detached during handling, such as the petrosal (NMS G.1992.47.121.2; Panciroli *et al.* 2018) and the dentary (NMS G.1992.47.121.3; Panciroli *et al.* 2019, 2021a).

NMS G.2020.4.1.1 comprises four parts containing the skeleton of *B. cuillinensis* (Fig. 2B). It measures approximately 8 cm by 6 cm, and <3 cm in depth. The original specimen recovered in the field was much larger (approximately 35 cm by 30 cm by 15 cm) and was iteratively reduced in size to obtain successful scans at high resolution for study (see above). All offcuts (including those not containing bone) were retained. Some bones are visible on the surface (left dentary, occipital condyles, parts of the ribs and metacarpals), but most of the skeleton is below the surface and only visible in the CT-data (Panciroli & Benson 2021).

### Axial skeleton

*Atlas arches.* Both half neural arches of the atlas (C1) are preserved in NMS G.1992.47.121.1 (Fig. 7A–H) and the left arch is preserved in NMS.G.2020.4.1.1 (Fig. 8A–D). In the former the two halves are located on opposite sides of the palate and majority of cranial elements (Fig. 1B), whereas in the latter the arch is next to the humerus (Fig. 2B). They are intact, with dorsoventrally tall dorsal arches that are convex laterally, and a small ventrolateral projection, resembling closely the morphology of the half



**TABLE 5.** Landmarks used in PCA analyses.

Skeletal element	Landmark/semilandmark
Scapula	L2. Point of maximum curvature of the anterior edge of scapular neck
	L3. Point of maximum curvature of the posterior edge of scapular neck
	L5. Ventral tip of the acromion process
	SL2. Edge of glenoid fossa; closed row
Humerus	L1. Most posterior point of greater tuberosity
	L2. Intersection of pectoral and deltoid crests
	L3. Most proximal point of deltoid crest
	L4. Most anterior point of lesser tuberosity
	L5. Most posterior point of lesser tuberosity
	L6. Proximal origin of lateral epicondylar crest
	L8. Most medial point of medial epicondyle (entepicondyle)
	SL1. Edge of the articular surface of humeral head; closed row
Ulna	SL2. Proximal edge of greater tuberosity followed by the edge of pectoral crest; from L1 to L2
	SL3. Edge of deltoid crest; from L2 to L3
	SL4. Medial edge of lesser tuberosity; from L4 to L5
	SL6. Edge of distal articular surface; closed row
	L1. Most proximal point of olecranon process
	L2. Most anterior point of olecranon process
Radius	L3. End of the proximal epiphysis in the medial edge; defined as the perpendicular point to L5 in the medial side
	L4. End of the proximal epiphysis in the lateral edge; defined as the perpendicular point to L5 in the lateral side
	L5. Point of maximum curvature in the distal base of coronoid process; this landmark defines the position of L3 and L4
	L6. Most anterior point of distal epiphysis
	SL1. Medial edge of olecranon process; from L2 to L3
	SL2. Lateral edge of olecranon process; from L2 to L4
Pelvis	SL3. Edge of proximal articular surface; closed row
	L1. Proximal tip of coronoid process
Femur	SL1. Edge of proximal articular surface; from L1 to L1
	L1. Intersection of ventral and anterior edges of iliac crest
	L2. Posterior end of the dorsal edge of iliac crest
	SL1. Anterior and dorsal edge of iliac crest; from L1 to L2
	SL3. Edge of distal articular surface; closed row

arches of the atlas in *Morganucodon* ('*Eozostrodon*'); Jenkins & Parrington 1976). The articular areas for the occipital condyle and atlas are preserved, the former being slightly larger than the latter, and both oval in shape and slightly concave. There is a strong medially directed projection where the two articular areas meet. The centrum

of the atlas (C1) is not preserved in either specimen of *Borealestes*, consistent with the fact that the half neural arches are not fused at the dorsal midline. The dentition of both specimens shows no sign of ongoing tooth replacement, the posteriormost molars have erupted in both specimens, and the posteriormost molar is aligned with the coronoid process. These are all adult features of other mammaliaforms and docodontans, therefore these specimens are adult individuals (for further support that these represent adult specimens see Discussion). Therefore the lack of fusion of components of the atlas is an adult character of the vertebrae, at least for *Borealestes*, as also interpreted for *Morganucodon* by others (Jenkins & Parrington 1976).

*Vertebrae.* In NMS G.1992.47.121.1 there are two cervical, three thoracic and four caudal vertebrae preserved (Fig. 7I–Q). None are completely preserved. In addition, there are two chevrons (haemal arches), one almost complete and the second a smaller, worn fragment (Fig. 7R–S). The post-axial cervical vertebrae of NMS G.1992.47.121.1 are represented only by their centra (Fig. 7I–J). The exact position of these vertebral centra in the vertebral column is uncertain, but one is noticeably smaller than the other and may be cervical 2 or 3, while the larger is more likely to be cervical 3 or 4. The centra are amphicoelous, oval when viewed anteriorly or posteriorly. The bases of the neural arch can be discerned on both vertebrae, but the arch and the dorsal portion of the vertebrae are not preserved. Both vertebrae are slightly distorted, but it is clear they are only slightly longer anteroposteriorly than they are wide mediolaterally. The middle part of the centrum is bilaterally constricted on both. There is one possible cervical vertebra in NMS.G.2020.4.1.1, but it is represented only by a fragment of the right transverse process and neural arch (Fig. 8E). However, its position in the cervical series is not clear, and it could instead be a thoracic vertebra.

There are at least three thoracic vertebrae represented in NMS G.1992.47.121.1 (Fig. 7K–M). One thoracic vertebra shows a distorted and poorly preserved centrum lacking processes or arch; one vertebra has a preserved neural spine with transverse processes but no centrum; and the third has a dorsoventrally compressed almost complete vertebra, with centrum, arches and neural spine. Their exact position in the vertebral column is not certain. The centrum is badly distorted in both vertebrae preserved with a centrum, making the original shape difficult to interpret. It appears to be anteroposteriorly shorter than it is mediolaterally wide or dorsoventrally tall. As with the cervical vertebrae, it is amphicoelous and constricted at the middle part of the centrum, and shows a distinct rim around the edge of the centrum. The neural spines of

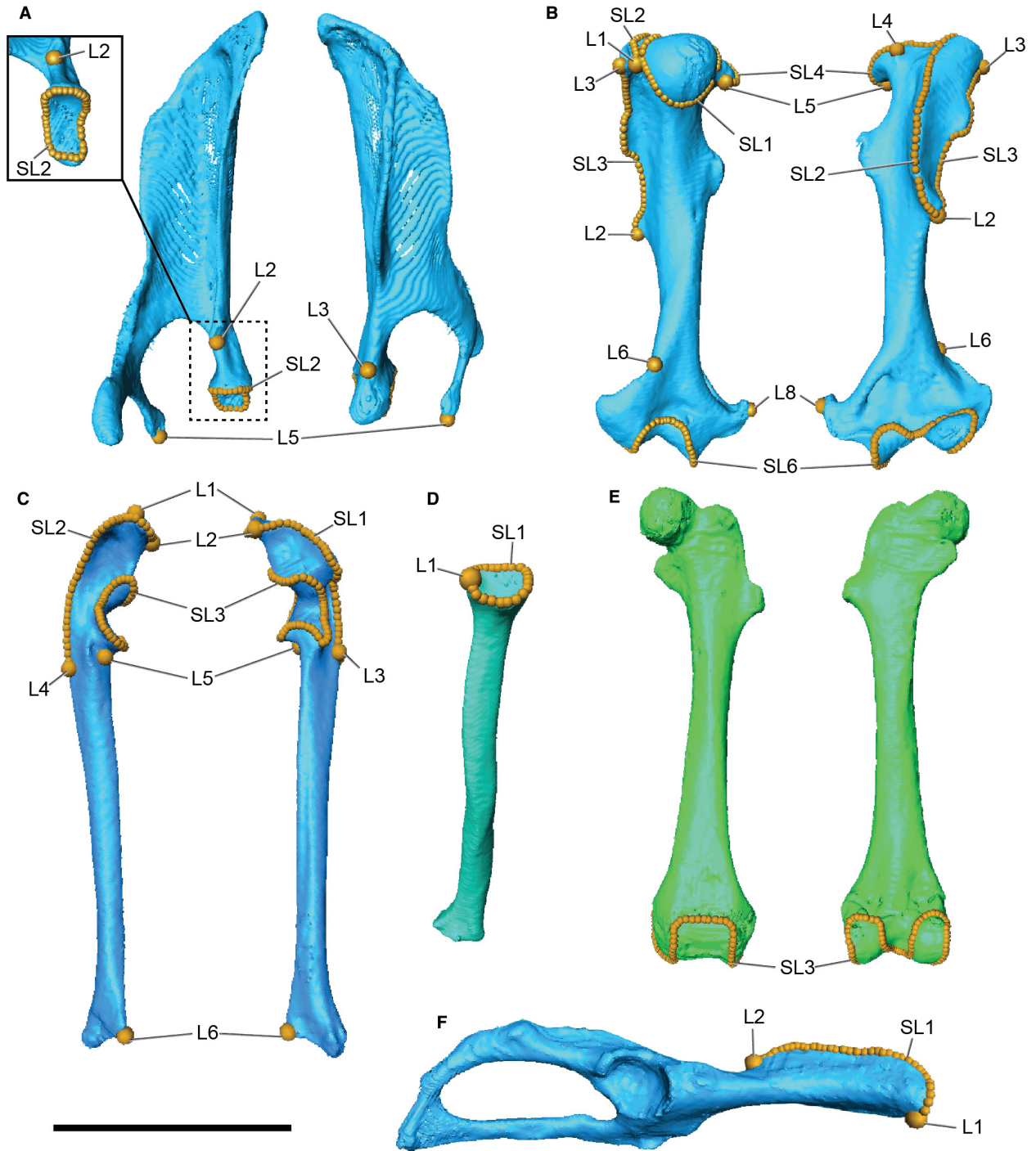


**FIG. 3.** 3D landmarks and semilandmarks used in principal components analysis. A, scapula. B, humerus. C, ulna. D, radius. E, femur. F, pelvis. Postcrania of *Diplomesodon pulchellum* shown as example. Scale bar represents 10 mm.

the thoracic vertebrae are long and slant diagonally posteriorly from the neural arch (Fig. 7L–M). The postzygapophyses are at the base of the neural arch, and on the right side of one vertebra the articular facet for the rib is preserved, posterolateral to the base of the prezygapophysis (which is not preserved). The neural canal is

preserved in the largest of the vertebrae, but it is compressed.

The six thoracic vertebrae preserved in *B. cullinensis*, NMS.G.2020.4.1.1 are all incomplete (Fig. 8F–K), but the two largest are relatively complete, although compressed dorsoventrally (Fig. 8J–K). Their centra, neural spines

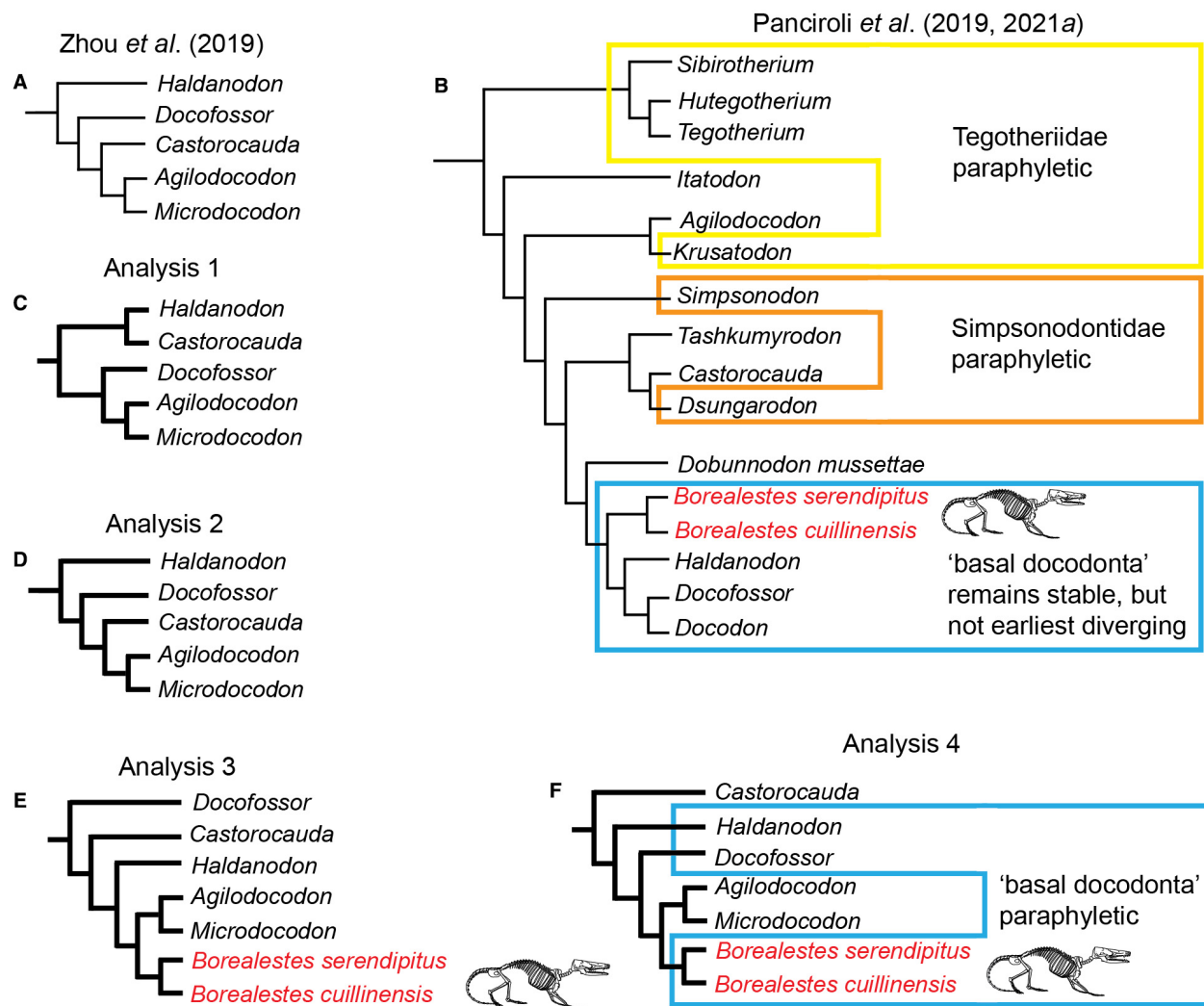


**FIG. 4.** Results of phylogenetic analyses of docodontans using: A, dental, cranial and postcranial characters from Zhou *et al.* (2019); B, dental and cranial characters presented in Panciroli *et al.* (2021a), based on analysis originally published in 2019); C, Zhou *et al.*'s (2019) original matrix (which did not include *Borealestes*); D, Zhou *et al.*'s (2019) original matrix, with modified parameters (see Material and Method), without *Borealestes*, but amending characters scores for characters 32, 56, 67, 127, 131, 133, 312, 362 and 522 for docodontans, where our interpretation differed from the previous authors' (see Supporting Information); E, Zhou *et al.*'s (2019) original matrix with *Borealestes* species added; F, as for Analysis 3 (E), adding *Borealestes* species. See Material and Method, and Supporting Information, for full details of analyses.

and transverse processes resemble those in NMS G.1992.47.121.1. The largest of the thoracic vertebrae in NMS.G.2020.4.1.1 (Fig. 8K), is probably from a more posterior position in the thoracic series than the others, based on its size.

No caudal vertebrae are preserved in *B. cuillinensis*, but in *B. serendipitus* there are four: one proximal (Fig. 7N), one from a position distal to this (Fig. 7O), and two from still further along the tail length (Fig. 7P–Q). The most proximal caudal vertebra is incomplete, comprising the left transverse process, a portion of the centrum, and the base of the incomplete right transverse process. The centrum is compressed dorsoventrally, and lacks the dorsal and

ventralmost portions, including the base of the neural arch. The size and structure of this vertebra suggests that it is from the proximal section of the tail, probably one of caudals 3–7. The preserved transverse process projects quite far laterally, similar to the proximal caudals of *Microdocodon* (Zhou *et al.* 2019) and also somewhat similar to that seen in *Castorocauda* (Ji *et al.* 2006) but less extreme.

The next vertebra preserved in the caudal series in *B. serendipitus* is from mid-way along the tail, probably between caudals 8 and 12 (Fig. 7O). It is amphicoelous and strongly constricted at the midline, especially dorsoventrally. It is longer anteroposteriorly than it is wide mediolaterally, presenting a rectangular profile in dorsal and ventral view.

**TABLE 6.** Results of principal components analysis on postcranial elements.

	PC1	PC2	PC3
<b>Humerus</b>			
Standard deviation	0.095172	0.060462	0.042376
Proportion of variance	0.47198	0.19049	0.09357
Cumulative proportion	0.47198	0.66247	0.75604
<b>Pelvis (Ilium)</b>			
Standard deviation	0.101515	0.098648	0.078901
Proportion of variance	0.30401	0.28707	0.18365
Cumulative Proportion	0.30401	0.59108	0.77473
<b>Femur</b>			
Standard deviation	0.134643553	0.065358733	0.051291991
Proportion of variance	0.50577	0.11918	0.0734
Cumulative proportion	0.50577	0.62495	0.69834
<b>Scapula</b>			
Standard deviation	0.176054	0.113473	0.086716
Proportion of variance	0.42548	0.17675	0.10322
Cumulative proportion	0.42548	0.60223	0.70546
<b>Ulna</b>			
Standard deviation	0.19311	0.069193	0.059101
Proportion of variance	0.62958	0.08083	0.05897
Cumulative proportion	0.62958	0.71041	0.76938
<b>Radius</b>			
Standard deviation	0.114379	0.094099	0.054644
Proportion of variance	0.39695	0.26867	0.0906
Cumulative proportion	0.39695	0.66562	0.75622

First three PCs only; for complete results see Supporting Information.

There is no neural canal. The ventral side is smooth and convex, while the dorsal side of the vertebra has a strong ridge running anteroposteriorly, flanked by deep indentations laterally. There are no complete preserved transverse processes or zygapophyses, although there appears to be the base of a possible zygapophysis on the dorsal surface of the vertebra at the posterior and anterior ends.

The two distalmost caudal vertebrae comprise one posterior end of a vertebra (Fig. 7P) and a second almost complete vertebra (Fig. 7Q), probably from somewhere between caudals 14 and 18, by comparison to *Microdocodon* (Zhou *et al.* 2019). They are positioned together on the surface of the limestone block, beside the fragments of the left dentary and left humerus (Fig. 1A). The almost complete caudal vertebra is much longer anteroposteriorly than it is wide mediolaterally. It is damaged on the right anterior side, and what is preserved on the left includes a distinct ridge, projecting dorsolaterally. There is no corresponding projection on the poster end of the vertebra. The less complete vertebra matches the morphology of the posterior portion of the more complete vertebra, and was therefore likely to have originally been of similar proportions and shape. Both of the posteriormost caudal vertebrae have a smooth ventral surface, and a ridge along the dorsal surface. Unlike in the caudal 8–12 vertebrae,

this ridge comprises most of the body of the bone, with no lateral indentations. The vertebrae flare bilaterally at the anterior and posterior ends, forming mediolaterally wide articulation surfaces with the next vertebra. Unlike the other vertebrae described here for *Borealestes*, there is no concavity on the centrum.

*Chevrons.* The two chevrons preserved in *B. serendipitus*, NMS G.1992.47.121.1, are very different in size, the larger and more complete chevron coming from a more anterior position and the smaller from a distal position on the tail (Fig. 7R–S). The smaller chevron is part of the main limestone block, positioned near the main portion of the skull, whereas the larger chevron, NMS G.1992.47.121.8, was dislodged from the main block and scanned separately. NMS G.1992.47.121.8 is almost intact, and is diamond shaped when viewed dorsally or ventrally (Fig. 7R). It flares laterally at the midline, and these flares project dorsally to their position between the caudal vertebrae, and enclose a dorsal canal along the anteroposterior length of the chevron. There is a protuberance at the elongated anterior end of the chevron (Fig. 7R), but damage makes it unclear if the same protuberance was present on the posterior end. By comparison to *Microdocodon*, the shape of this larger chevron is similar to those

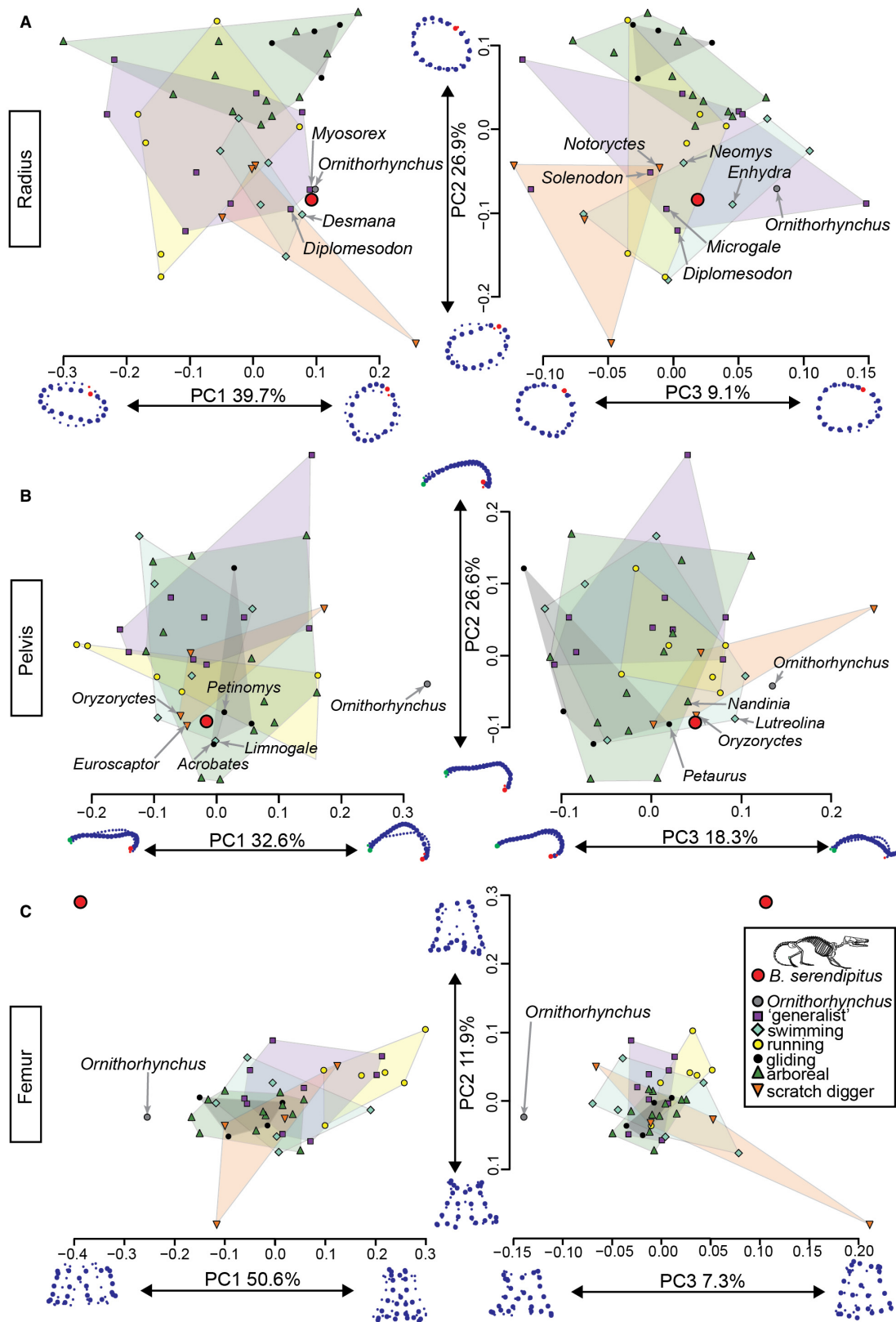


**FIG. 5.** Results of principal component analyses on select postcranial elements in NMS G.1992.47.121.1. A, radius; B, pelvis; C, femur. Legend same throughout. Shape deformation of landmarks shown on PC axes. For more information and full labelling of taxa, see Supporting Information.

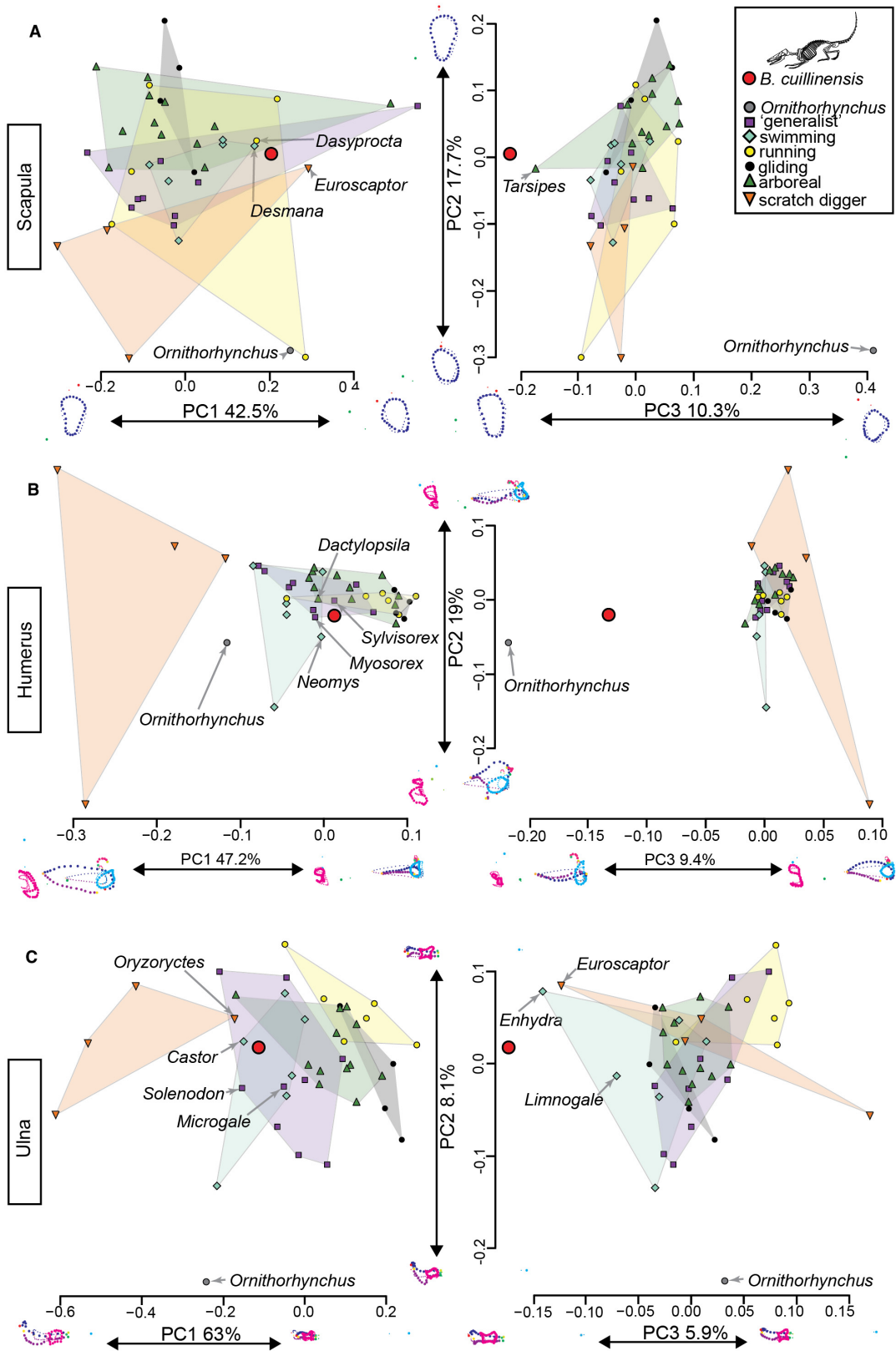


**FIG. 6.** Results of principal component analyses on select postcranial elements in NMS G.2020.4.1.1. A, scapula; B, humerus; C, ulna. Legend same throughout. Shape deformation of landmarks shown on PC axes. For more information and full labelling of taxa, see Supporting Information.



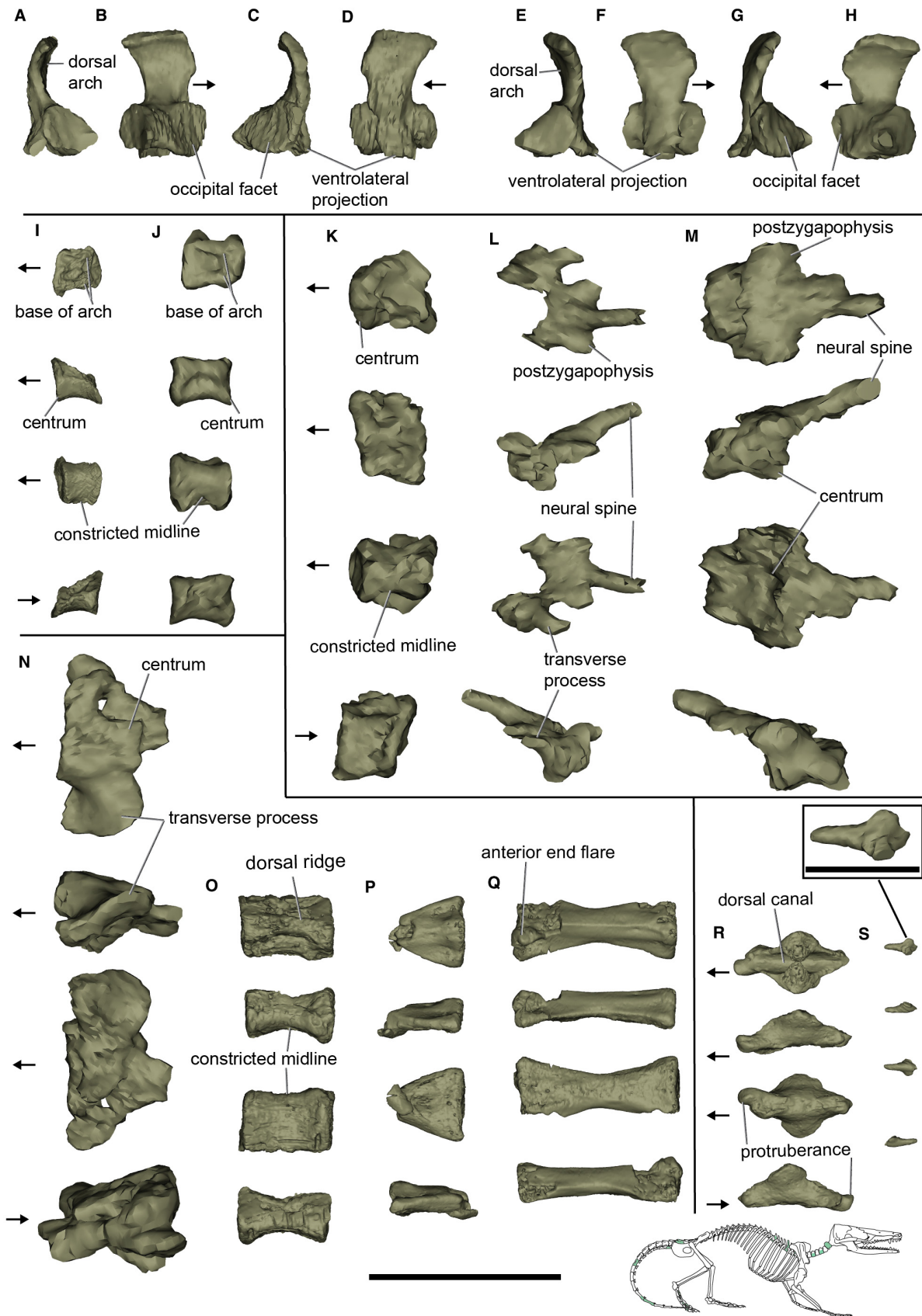


**FIG. 7.** Atlas arches, vertebrae and chevrons of NMS G.1992.47.121.1 (A–Q, S) and NMS G.1992.47.121.8 (R), *Borealestes serendipitus*. A–D, left atlas arch: A, posterior; B, medial; C, anterior; D, left lateral view. E–H, right atlas arch: E, posterior; F, right lateral; G, anterior; H, medial view. I–J, cervical vertebrae. K–M, thoracic vertebrae. N–Q, caudal vertebrae. R–S, chevrons. In I–S vertebrae are pictured from top to bottom in: dorsal; left lateral; ventral; and right lateral view. Scale bars represent: 5 mm for all main images; 1 mm on enlargement of S.

between caudals 6 and 9 in that taxon (Zhou *et al.* 2019, fig S11C–D).

The smaller chevron, part of NMS G.1992.47.121.1, comprises only a small projection and the central body of the chevron (Fig. 7S). Although superficially resembling a claw, the flared main body of the bone is mediolaterally broad, making it different from ungual morphology. The small size suggests it was a distal chevron from beyond the middle part of the caudal vertebral series.

*Ribs and clavicle.* There are at least nine ribs preserved in NMS G.1992.47.121.1 (Figs 1A–B, 9A–B), with a rib fragment separated from the rest of the skeleton (NMS G.1992.47.121.12, Fig. 9C). There are approximately eight preserved in NMS.G.2020.4.1.1 (Fig. 9E, F). The ribs are similar in both species, resembling those in most other docodontans for which the ribs are known, but lacking the flattened appearance seen in *Castorocauda* (Ji *et al.* 2006).

A portion of the right clavicle, NMS G.1992.47.121.6, is separated from the main limestone block (Fig. 9D). The lateral end is slightly concave, and would have articulated with the acromion on the scapulacoracoid (not present in this specimen). The medial end of the clavicle that would have articulated with the interclavicle is missing.

#### Appendicular skeleton

*Scapulacoracoid.* There is no scapulacoracoid preserved in *B. serendipitus*, NMS G.1992.47.121.1. The right scapulacoracoid is present in *B. cuillinensis*, NMS.G.2020.4.1.1, preserved next to the remnants of the skull (Figs 2B, 10). The preserved part consists of a nearly complete coracoid, the glenoid facet, and ventral part of the scapula that bears the intact acromion. The dorsal half of the scapula is missing, and was also damaged by the saw during extraction of the specimen (Fig. 10). What is preserved of the scapulacoracoid of *B. cuillinensis* resembles *Haldanodon* (Martin 2005). It shows a wide, saddle-shaped glenoid facet with an oval outline, relatively larger than the glenoid facet in *Microdocodon* (Zhou *et al.* 2019). The anterior margin of the scapula is strongly curved. The acromion forms the ventralmost part of the anterior scapular margin, and doesn't extend beyond the level of the margin of the glenoid facet, as in *Haldanodon*.

The scapula–coracoid suture runs through the dorsalmost portion of the glenoid facet (Fig. 10). The procoracoid and procoracoid foramen are absent in *Borealestes*,

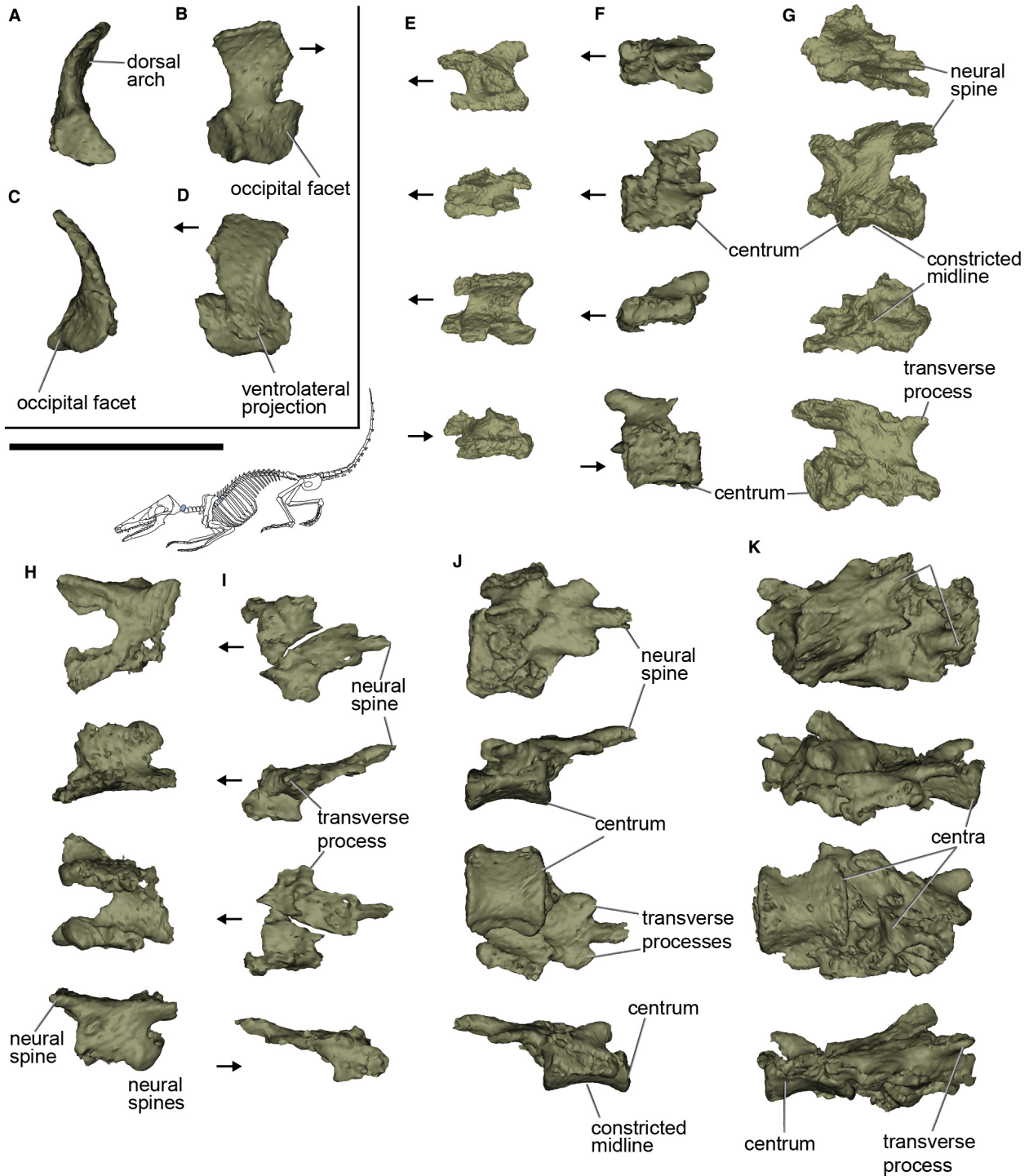
as in *Haldanodon* (Martin 2005). The coracoid consists of a glenoid component and a peg-like coracoid process. The ventral margin of the glenoid is marked by a crest and there is a tubercle, which we interpret as the attachment area of the coracobrachialis muscle. The ventralmost tip of the coracoid process would be for the origination of the biceps brachii, it is either damaged, or its tip was not ossified and therefore not fossilized in NMS.G.2020.4.1.1. A similar muscle attachment pattern was also interpreted for the cynodont *Massetognathus* (Lai *et al.* 2018). This corresponds to the muscle pattern of the living monotremes (Gambaryan *et al.* 2015). The coracoid process flares slightly at the end where the coracoid head of the triceps would have attached in life.

*Humerus.* An almost complete humerus is preserved in *B. cuillinensis* NMS.G.2020.4.1.1, located near the atlas arch and some scattered metacarpals/tarsals (Figs 2B, 11E–H). Only a fragment of the deltopectoral crest of the left proximal humerus is present in *B. serendipitus*, NMS G.1992.47.121.1, located beside the fragment of posterior left dentary (Figs 1B and 11A–D). The abraded broken surface of this fragment of humerus suggests that the bone may have been complete on the surface of the limestone, but was either broken or eroded prior to collection.

The deltopectoral crest of *B. serendipitus* appears larger than in *B. cuillinensis*, with a deep fossa for muscle insertion (Fig. 11). However, this may be due to the broken and slightly crushed position of the deltopectoral crest in this specimen of *B. cuillinensis*, and may not be a true difference between the species. What remains of the greater tubercle and humeral head in *B. serendipitus* indicates a relatively large head, but there is too little preserved to indicate further details of its morphology.

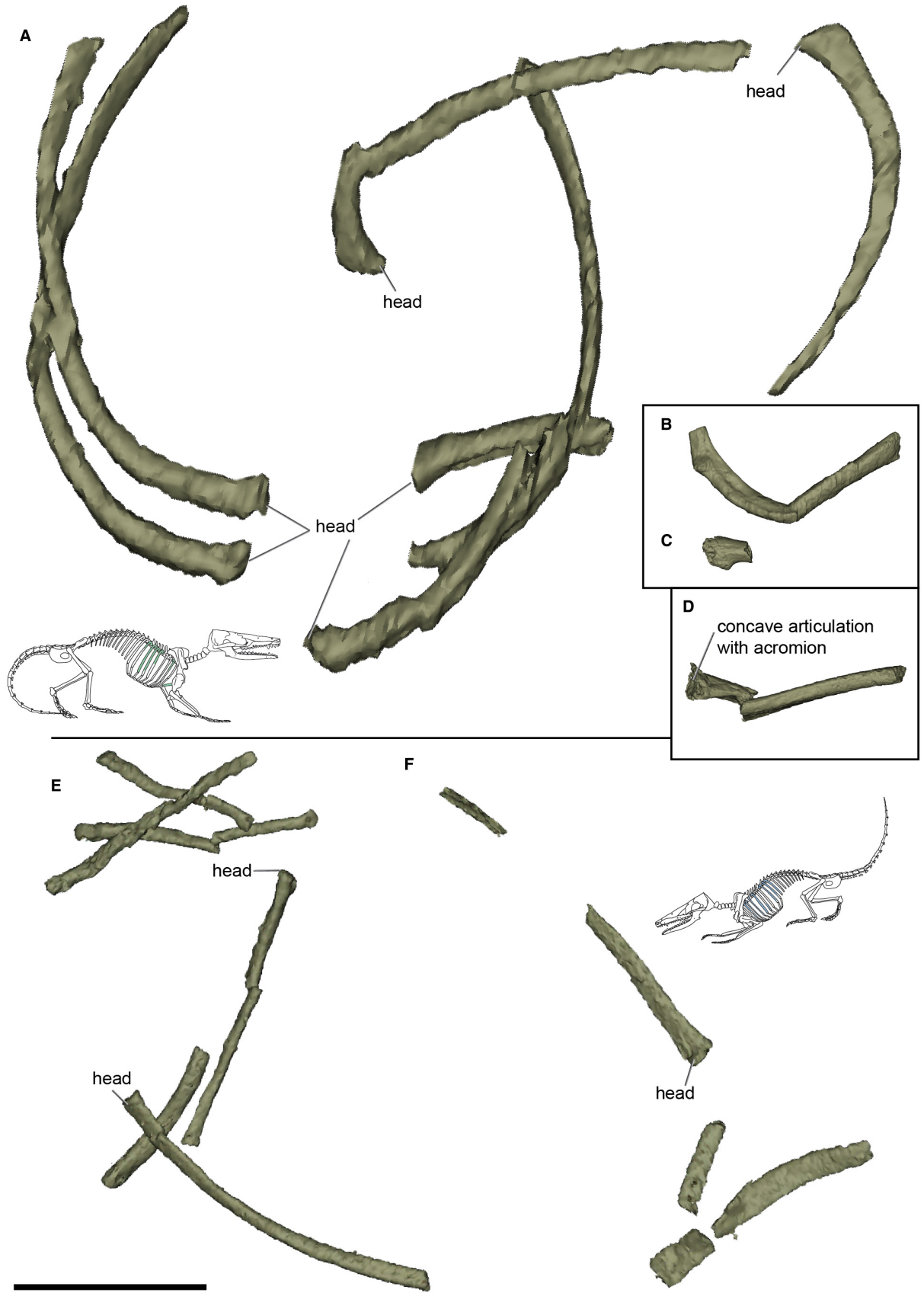
In NMS.G.2020.4.1.1 (*B. cuillinensis*) most of the humerus is preserved, with only a small section of the deltopectoral crest and the ectepicondyle missing (Fig. 11E–H). It is relatively shorter and more robust bone than those of *Agilodocodon* (Meng *et al.* 2015) or *Microdocodon* (Zhou *et al.* 2019) but less robust than that seen in *Haldanodon* (Martin 2005). The greater tubercle is larger than the lesser tubercle, and the deltopectoral crest is less developed on the lateral aspect of the humerus in *B. cuillinensis* than in *Haldanodon*, and terminates halfway down the humeral shaft. Below the lesser tubercle, the teres major tuberosity is well developed on the medial side of the humerus. The humerus has the same 'hourglass shape' as *Haldanodon* (Martin 2005,





**FIG. 8.** Atlas arches and vertebrae of NMS G.2020.4.1.1, *Borealestes cuillinensis*. A–D, left atlas arch: A, posterior; B, medial; C, anterior; D, left lateral view. E, cervical vertebra. F–K, thoracic vertebrae. In E–K vertebrae are pictured from top to bottom in: dorsal; left lateral; ventral; and right lateral view. Scale bar represents 5 mm for all elements.

**FIG. 9.** Ribs and clavicle of *Borealestes serendipitus* (A–D) and *B. cuillinensis* (E, F). A–B, NMS G.1992.47.121.1: A, ribs as in position in matrix; B, rib from elsewhere in matrix. C, rib fragment NMS G.1992.47.121.12. D, right clavicle NMS G.1992.47.121.6. E–F, ribs belonging to NMS G.2020.4.1.1: E, cluster of ribs from part AA (see Fig. 2B); F, cluster of ribs from part CC. Scale bar represents 5 mm for all elements.



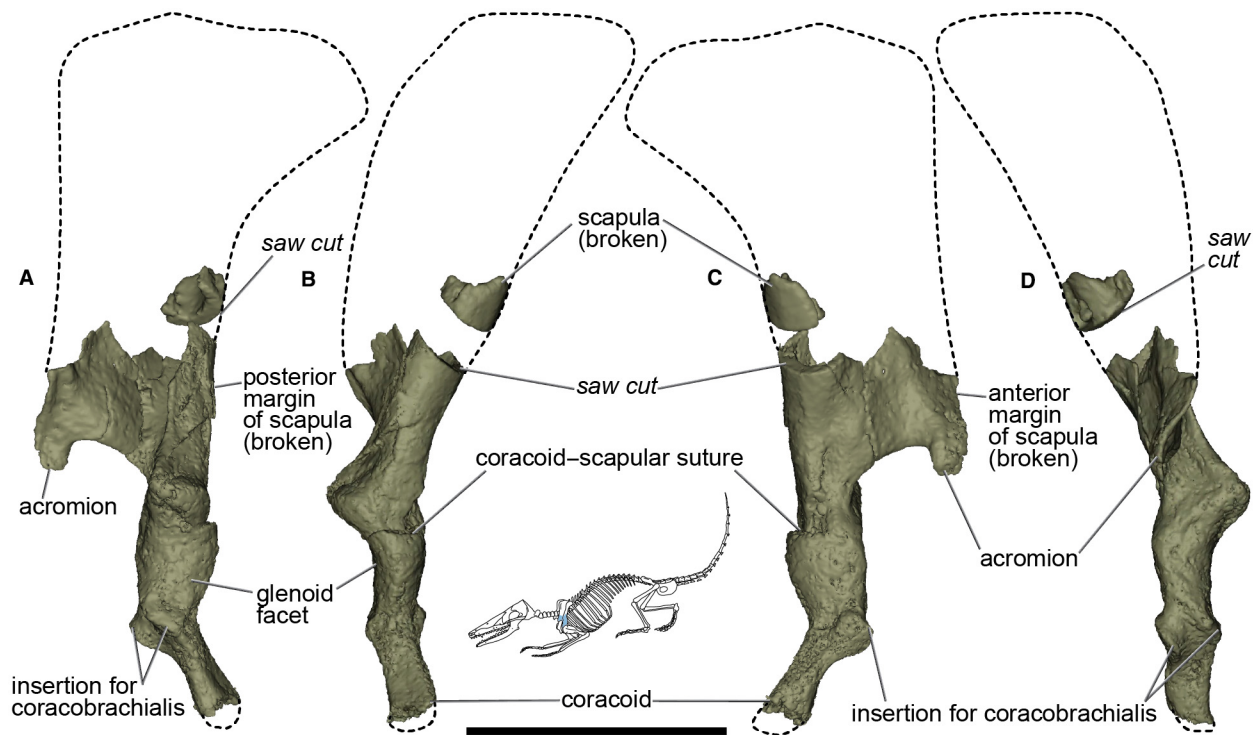


**FIG. 10.** Scapulacoracoid of NMS G.2020.4.1.1, *Borealestes cuillinensis*. A, medial; B, anterior; C, lateral; D, posterior view. Scale bar represents 5 mm.

p. 227), caused by the expanded proximal and distal ends of the bone and twisting of the ends relative to one another, known as humeral torsion (Gambaryan & Kielan-Jaworowska 1997; Luo & Wible 2005), a common feature of mammaliaforms, and some crown mammals. The distal end is broad, but less so compared to the humeral length than seen in *Haldanodon* (approximately 57% of humeral length, vs 61.3% in *Haldanodon*; Martin 2005, p. 227). The radial condyle is spherical and large, and the ulnar condyle is smaller and mediolaterally compressed. The large entepicondyle suggests a well-developed area of muscle attachment, for origination of flexor muscles of the wrist and digits, and for flexion and pronation of forearm, by comparison with extant mammals (Evans & de LaHunta 2012; Gambaryan *et al.* 2015; Regnault *et al.* 2020).

**Radius.** The left radius of *B. serendipitus* is preserved on the surface of the limestone block in specimen NMS G.1992.47.121.1 (Figs 1A, 12A–D). It is complete with only the distalmost end missing (Fig. 12A–D). There is a relatively wide, cup-shaped and projecting articular fovea, strongly sloping medially in dorsal view.

The radius is somewhat sigmoidal along its length, and in intact anatomy would be positioned alongside the ulna. The ulna is not preserved in NMS G.1992.47.121.1. The

distal end of the radius is somewhat expanded, but does not appear to be transversely wider than the proximal end, although the missing styloid process makes this interpretation uncertain. A ridge runs along the distal half of the length of the shaft on the dorsal side, somewhat laterally positioned. This blends smoothly into a groove on the lateral side of the distal radius. This groove would run to the styloid process, but this process is broken and missing. Medially, a much smaller groove is visible on the mediadorsal surface of the distal end of the radius. The long slender morphology resembles the radius of *Microdocodon* (Zhou *et al.* 2019, fig S10) and *Agilodocodon* (Meng *et al.* 2015), rather than the more robust (relatively wider and shorter) morphology of *Haldanodon* (Martin 2005) and *Docofossor* (Luo *et al.* 2015a).

**Ulna.** No ulna is preserved in *B. serendipitus*, but an almost complete left ulna, and proximal portion of right ulna, are preserved in *B. cuillinensis*, NMS.G.2020.4.1.1 (Figs 2B, 12E–L). The left ulna was damaged during extraction of the skeleton, removing a small portion of the shaft of the bone during cutting (Fig. 12E–H). The width of the saw blade is known (*c.* 1 mm), so the length of the ulna can be reconstructed reliably. The olecranon process is well developed. Its proximal ventral margin (or dorsal if oriented vertically) curves strongly dorsally (Fig. 12E–L),

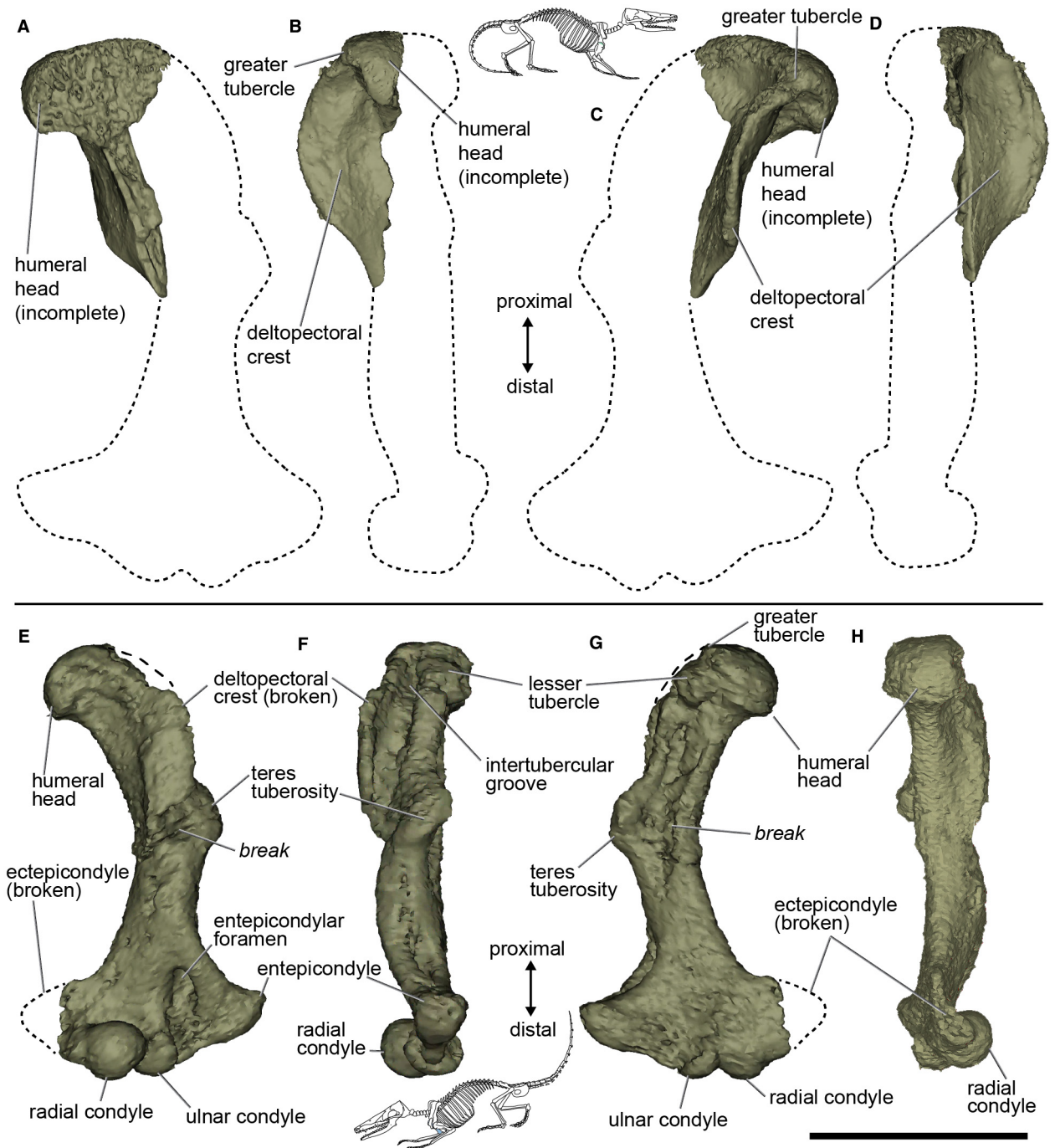


**FIG. 11.** Humerus of *Borealestes* species. A–D, left humerus of NMS G.1992.47.121.1, *B. serendipitus*: A, posterior; B, lateral; C, anterior; D, medial view. E–H, right humerus of NMS G.2020.4.1.1, *B. cuillinensis*: E, anterior; F, medial; G, posterior; H, lateral view. Scale bar represents 5 mm for all elements.

more so than in other mammaliaforms, a feature typical of other docodontans (Fig. 12M) (Martin 2013; Zhou *et al.* 2019, suppl. mat.) The olecranon has a rugose proximal surface for tendon insertion. The coronoid process is smaller and the semilunar notch is shallower and smaller than in *Haldanodon* (Martin 2005, 2013) or *Docofossor* (Luo

*et al.* 2015a), but larger than in *Microdocodon* (Zhou *et al.* 2019). The radial notch is distinct and the styloid process is concave and flared around the rim. The size of the ulna compared to the radius cannot be ascertained for either species of *Borealestes* because neither specimen includes both bones for comparison.



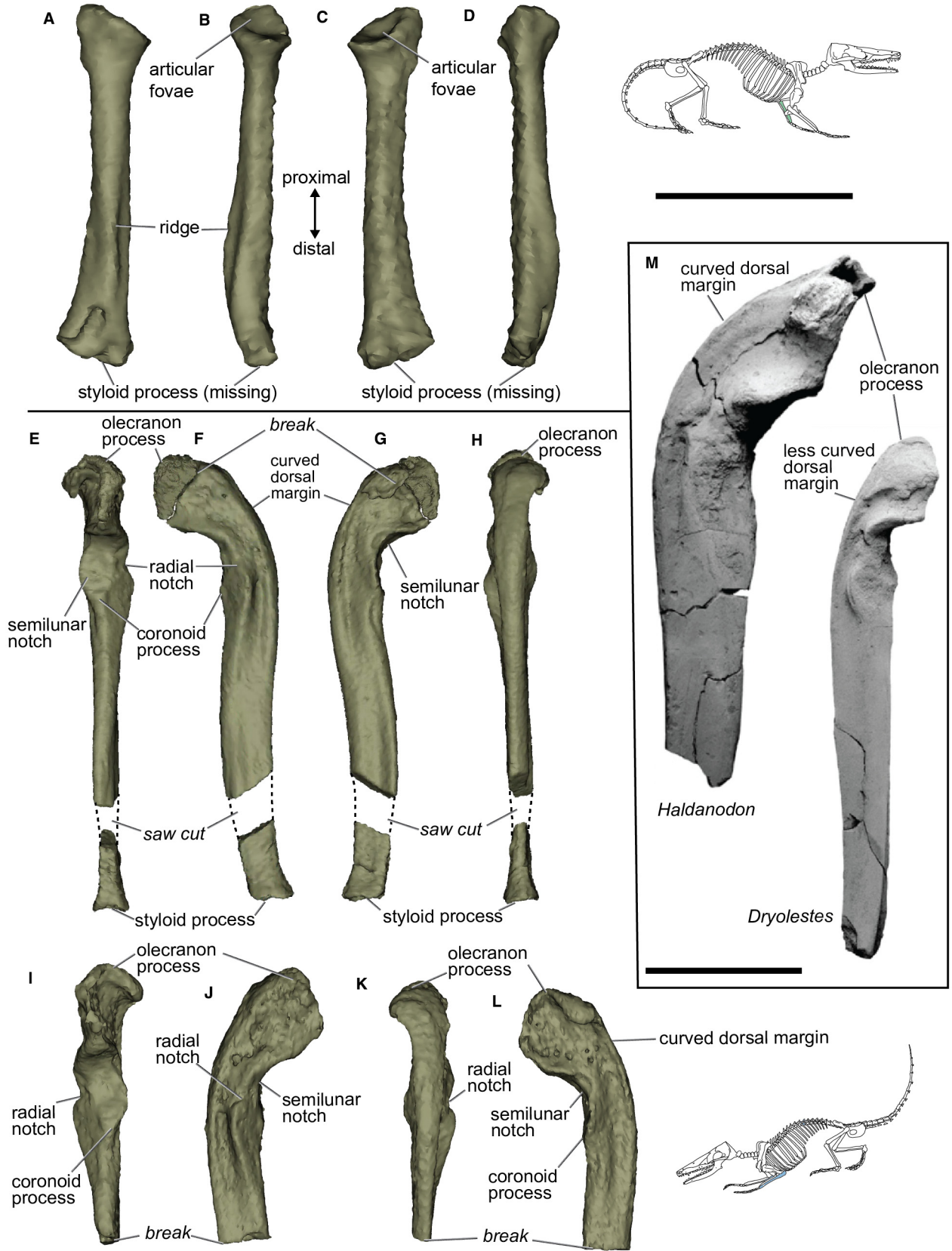


**FIG. 12.** Radius and ulna of *Borealestes* species. A–D, left radius of NMS G.1992.47.121.1, *B. serendipitus*: A, anterior; B, medial; C, posterior; D, lateral view. E–L, ulnae of NMS G.2020.4.1.1, *B. cuillinensis*: E–H, left ulna in: E, medial; F, anterior; G, posterior; H, lateral view; I–L, right ulna in: I, medial; J, anterior; K, lateral; L, posterior view. M, ulnae of *Haldanodon* and *Dryolestes* for comparison of dorsal (proximal) margin of the olecranon process (from Martin 2013, figs 2J, 3B). Scale bars represent 5 mm (A–L all same scale).

*Ilium.* The right ilium of *B. serendipitus* is preserved on the surface of the limestone block NMS G.1992.47.121.1, and is almost complete (Figs 1A, 13C–F). Overall the ilium appears similar to the described ilia of other docodontans in which it is known: the element is elongate, and the iliac blade is flattened laterally, but convex medially. There is a thin flange on the dorsal edge of the iliac blade, projecting dorsally from midway along the ilium and narrowing slightly anteriorly (Fig. 13C–E). The ventral edge of the anterior end of the iliac blade is also mediolaterally thin, and has no discernible bulging along the rim. There is no discernible rugose ilio-sacral contact on the medial side of the ilium, but some ghosting in the original tomographic slices makes it unclear. Overall, the ilium blade of *B. serendipitus* is wider than the more gracile ilium of *Microdocodon* (Zhou *et al.* 2019) but much narrower than the robust ilium of *Haldanodon* (Martin 2005). *Borealestes* bears resemblance in the ilium to *Morganucodon* (Jenkins & Parrington 1976).

The acetabular facet is large, triangular when viewed posteriorly, and slightly convex (Fig. 13C). The surface is slightly angled anterodorsally. The preserved part of ilium shows that the suture between the ilium and ischium was not fused in the adult. The articulation with the ischium is damaged; a small piece is broken and missing (Fig. 13C, E), most likely during collection or preparation of the specimen. The articulation with the ischium and pubis are evidently narrow, forming a shallow acetabular facet for the femoral head. Although the cotylar notch on the dorsal aspect of the acetabulum is well documented in other docodontans (Martin 2005; Zhou *et al.* 2019), it is not feasible to estimate this notch in *Borealestes* because the posterior part of the ilium and the acetabulum as a whole are not preserved in this specimen.

*Ischium.* The bone fragment NMS G.1992.47.121.11 is identified as the dorsal corner of the right ischial blade, the only part of the ischium preserved in this specimen of *B. serendipitus* (Fig. 13A, B, G, H). There is a strong ischial tuberosity, more pronounced than in *Microdocodon* (Zhou *et al.* 2019), with a concave lateral surface of the ischium. The dorsal edge of the ischium appears wide and flattened, sloping medioventrally (Fig. 13H).

*Femur.* An incomplete right femur is preserved in this specimen of *B. serendipitus* NMS G.1992.47.121.1, located at the opposite end of the limestone block from the rest

of the skeleton, near the right ilium (Figs 1B, 13I–M). The distal portion of the femur is well preserved extending from below the third trochanter (trochanter not preserved). A fragment of the proximal portion of the femur is preserved near the broken and crushed end of the distal portion, and has been placed in approximate position in the reconstruction, but it does not preserve the proximal morphology.

The preserved morphology of the distal femur is slender and gracile, similar to *Agilodocodon* (Meng *et al.* 2015) and *Microdocodon* (Zhou *et al.* 2019). It lacks the broad profile of the distal femur formed by the lateral and medial condyles in *Haldanodon* (Martin 2005) and *Castorocauda* (Ji *et al.* 2006). The intercondylar fossa is distinct, and there is a noticeable medial condyle, but the lateral condyle is less distinct and neither condyles flare. The preserved diaphysis of the femur is slender, similar to those of *Agilodocodon*, and other mammaliaforms such as *Morganucodon* and *Megazostrodon* (Jenkins & Parrington 1976).

*Manus and pes.* There are multiple metacarpals, metatarsals and carpal and tarsal elements preserved in both specimens of *Borealestes*, but as none of these elements are in articulation, identification is hindered.

There are seven metacarpal/tarsals, and seven carpal/tarsal elements present in *B. serendipitus*, NMS G.1992.47.121.1 (and associated dislodged material) (Fig. 14). Most are preserved in the main block containing the partial skeleton, but three other autopodial elements were preserved separately (NMS G.1992.47.121.5 (Fig. 14C), NMS G.1992.47.121.7 (Fig. 14D) and NMS G.1992.47.121.10 (Fig. 14E)). Two elements are identified as metacarpals: metacarpal 4, by its distinctive proximal asymmetry (Fig. 14J) and metacarpal 5, which has distinctive distal asymmetry (Fig. 14L). The metacarpal 5 is wider and shorter than its counterpart of *Agilodocodon* (Fig. 14L), but not as wide as the block-like metacarpal 5 of *Docofossor* (Luo *et al.* 2015a), or the extremely short metacarpal 5 in haramiyidans (Meng *et al.* 2017). It appears that in *Borealestes* the morphology of metacarpal 5 does not indicate the locomotor specializations known in other mammaliaforms. One metatarsal can also be positively identified: NMS G.1992.47.121.5 is separated from the skeletal block and represents metatarsal 3 (Fig. 14C), recognizable from the compacted morphology of the proximal joint, and size (compared to other elements,

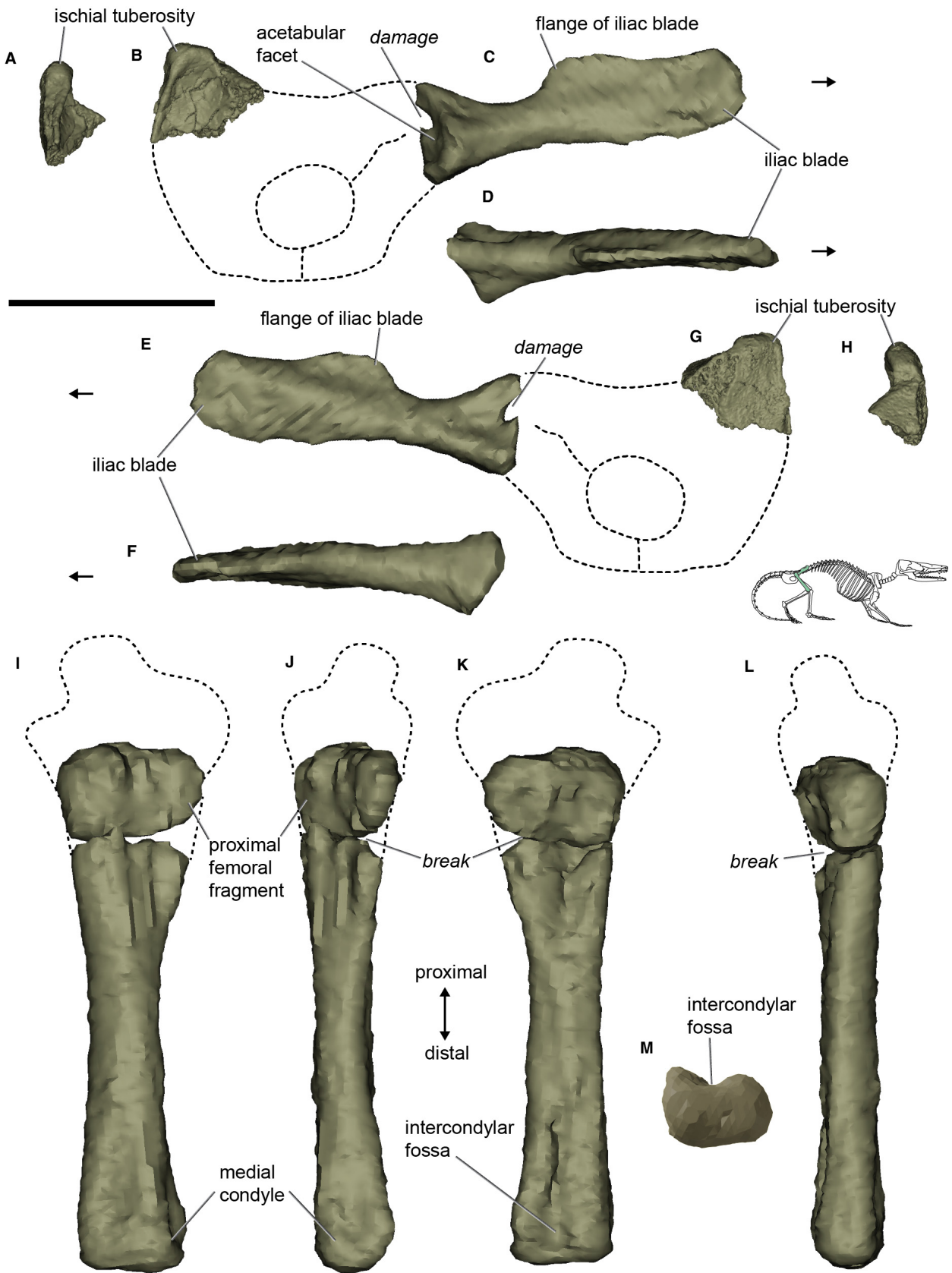


**FIG. 13.** Right ilium, ischium and femur of NMS G.1992.47.121.1, *Borealestes serendipitus*. A–B, G–H, NMS G.1992.47.121.11, ischial fragment: A, posterior; B, lateral; G, medial; H, dorsal view. C–F, ilium: C, lateral; D, dorsal; E, medial; F, ventral view. I–M, right femur: I, anterior; J, medial; K, posterior; L, lateral, M, distal view. Scale bar represents 5 mm for all elements.

and to those of *Agilodocodon*). All of these elements are identified by their resemblance to the corresponding elements in *Agilodocodon* (Meng *et al.* 2015). The remaining four autopodial elements lack distinctive features for the further identification, but their shorter length, with broader proximal end suggest that they are intermediate metacarpals or metatarsals. None of the metapodial bones show the epiphyseal suture, thus we interpret these finger bones as not having epiphyses, as in extant therians.

In NMS.G.2020.4.1.1 there are 11 metacarpals/metatarsals preserved, but none exhibit definitive identifiable features (Fig. 15B–L). There is also a single terminal phalanx, that would bear the horny claw in the intact animal (Fig. 15M), but it is not possible to tell if this is from the manus or pes. It resembles other docodontan unguals in shape, being mediolaterally narrow with a strong proximal overhanging process and a well-developed proximal flexor process. There is a lateral groove on either side of the claw for attachment of the claw sheath. The terminal phalanx is not bilaterally compressed as the terminal phalanx of *Agilodocodon* (Meng *et al.* 2015, fig. 3), a feature indicative of arboreal habits in *Agilodocodon* and other taxa (MacLeod & Rose 1993) *Borealestes*' terminal phalanx is suggestive of non-specialist locomotor modes (MacLeod & Rose 1993).

Of the seven carpal/tarsal in this specimen of *B. serendipitus*, two elements remain unidentified (Fig. 14E, F; NMS G.1992.47.121.10), but the remaining elements are identified as an entocuneiform (Fig. 14A), a cuboid (Fig. 14B), a probable navicular (Fig. 14D; NMS G.1992.47.121.7), right calcaneus (Fig. 16A–C) and right astragalus (Fig. 16D, E). The left entocuneiform has a well-formed entocuneiform–metatarsal saddle joint, facilitating movement of metatarsal 1. The cuboid also has a wide distal cuboid–metatarsal facet. The astragalus was positioned deep within the limestone block and as a result the resolution of the scan means surface detail is limited. However the tibio-astragalar trochlea and post-astragalar shelf are identifiable. They are less developed than in *Docofossor*, and like the rest of the pedal and manual elements there is no sign of the anatomical specializations for a fossorial lifestyle as seen in *Docofossor* (Luo *et al.* 2015a). Only two carpal/tarsal bones are preserved in NMS.G.2020.4.1.1, *B. cuillinensis*: one is identified as a probable lunate (Fig. 15A) and the other is a left calcaneus (Fig. 16G–I).

The calcanea of *Borealestes* exhibit almost identical morphology in both species. The right calcaneus in NMS G.1992.47.121.1, and is located near the ribs on the main

skeleton block, below the surface (Fig. 1B). In NMS.G.2020.4.1.1, a left calcaneus is located near the ulnae (Fig. 2B). In both species, the calcaneus is short and curved ventrally with a small calcaneal tuber (Fig. 16F). The morphology shows plesiomorphic features shared with other non-mammalian mammaliaforms such as *Morganucodon* (Jenkins & Parrington 1976; Szalay 1994; Zhou *et al.* 2013) and other docodonts for which the calcaneus is known, such as *Agilodocodon* (Meng *et al.* 2015), *Microdocodon* (Zhou *et al.* 2019) and *Docofossor* (Luo *et al.* 2015a). In *Borealestes* the calcaneus appears slightly less elongate than in *Agilodocodon*, being more similar to the morphology of *Morganucodon*. However, this might be attributed to the damage sustained on the calcaneal tuber of both *Borealestes* calcanea, which may make it appear less elongate. In NMS.G.2020.4.1.1, additional bony material is adhered to the tuber; this may be the displaced end of the tuber.

## DISCUSSION

### *Phylogenetic analysis*

All four of our analyses recover a docodontan subclade comprising *Borealestes* spp as the sister taxon to a clade of *Agilodocodon* + *Microdocodon* (Fig. 4C–F). The taxonomic scope here is limited to those taxa for which cranial and postcranial material is known. However, the two *Borealestes* species are recovered as sister taxa, a result that agrees with the analysis of the dentary and mandibular characters in Panciroli *et al.* (2019, 2021a) (Fig. 4B). Within Docodonta, the placement of *Castorocauda*, *Haldanodon* and *Docofossor* differs slightly between analyses, although these three taxa are consistently placed in various configurations as outgroups to *Borealestes* + (*Agilodocodon* + *Microdocodon*).

Because of its older geological age (Bathonian, compared to Oxfordian/Kimmeridgian for the other docodontan taxa), it might be expected that *Borealestes* would be an early-diverging member of the docodontan clade; *Borealestes* species therefore might be expected to represent the plesiomorphic character states for the clade. However, our tree topology of docodontan taxa differs significantly from that of Panciroli *et al.* (2021a), which employed a much larger sampling of docodontans that are preserved by dental and mandibular material only. That analysis recovered *Borealestes* species as sister to a clade comprising *Haldanodon* + (*Docofossor* + *Docodon*), all considered to be 'basal' docodontans, but it found this



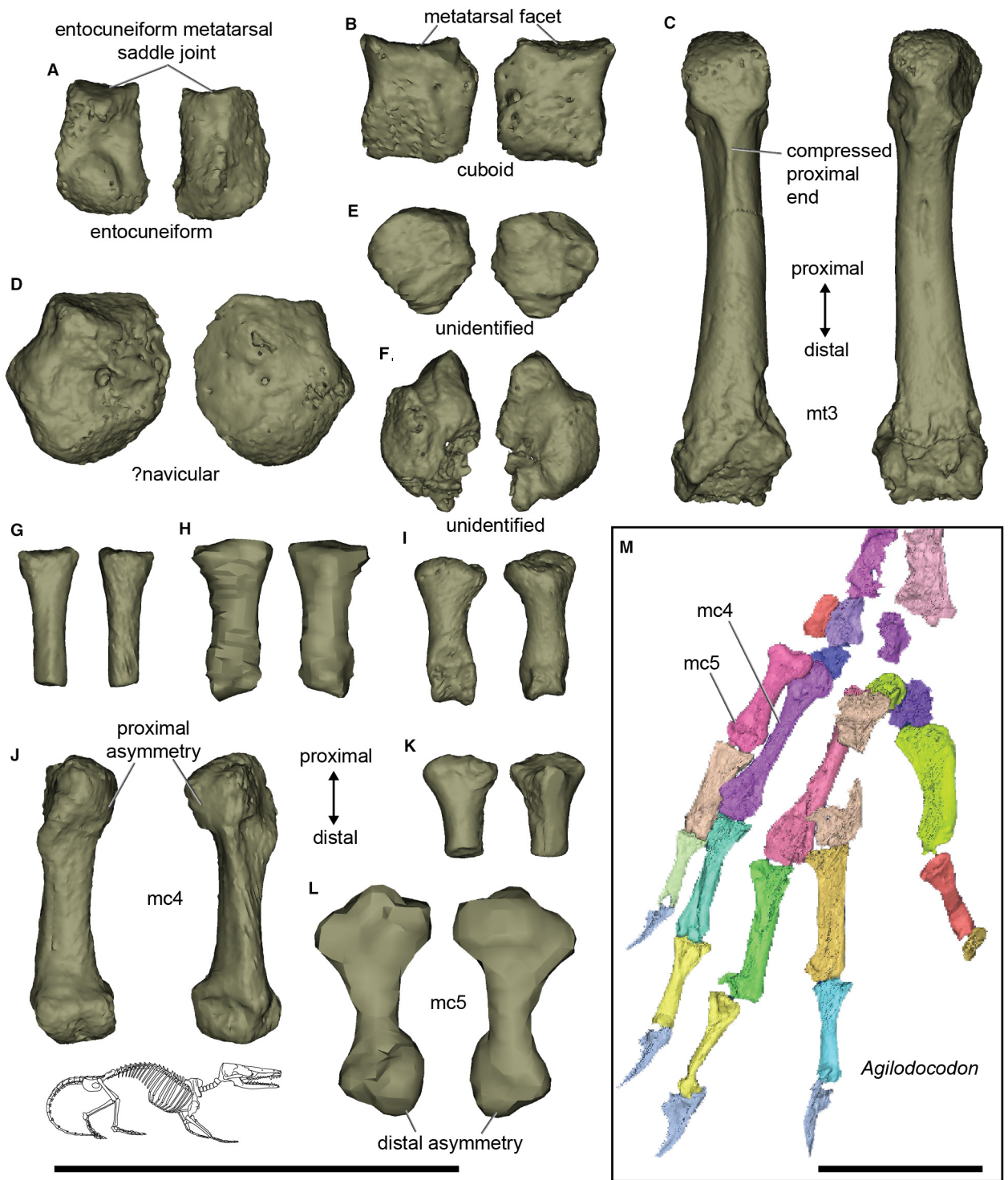


**FIG. 14.** Manus and pes elements of NMS G.1992.47.121.1, *Borealestes serendipitus*. A, entocuneiform. B, cuboid. C, metatarsal 3 (NMS G.1992.47.121.5). D, ?navicular (NMS G.1992.47.121.7). E, unidentified element (NMS G.1992.47.121.10). F, unidentified element. G–I, intermediate metacarpals/tarsals (mc/mt). J, metacarpal 4. K, intermediate metacarpal/tarsal. L, metacarpal 5. All elements shown in ventral (left) and dorsal (right) views. M, manus of *Agilodocodon* for comparison (from Meng *et al.* 2015, fig. S6). Scale bars represent 5 mm (A–L all same scale).

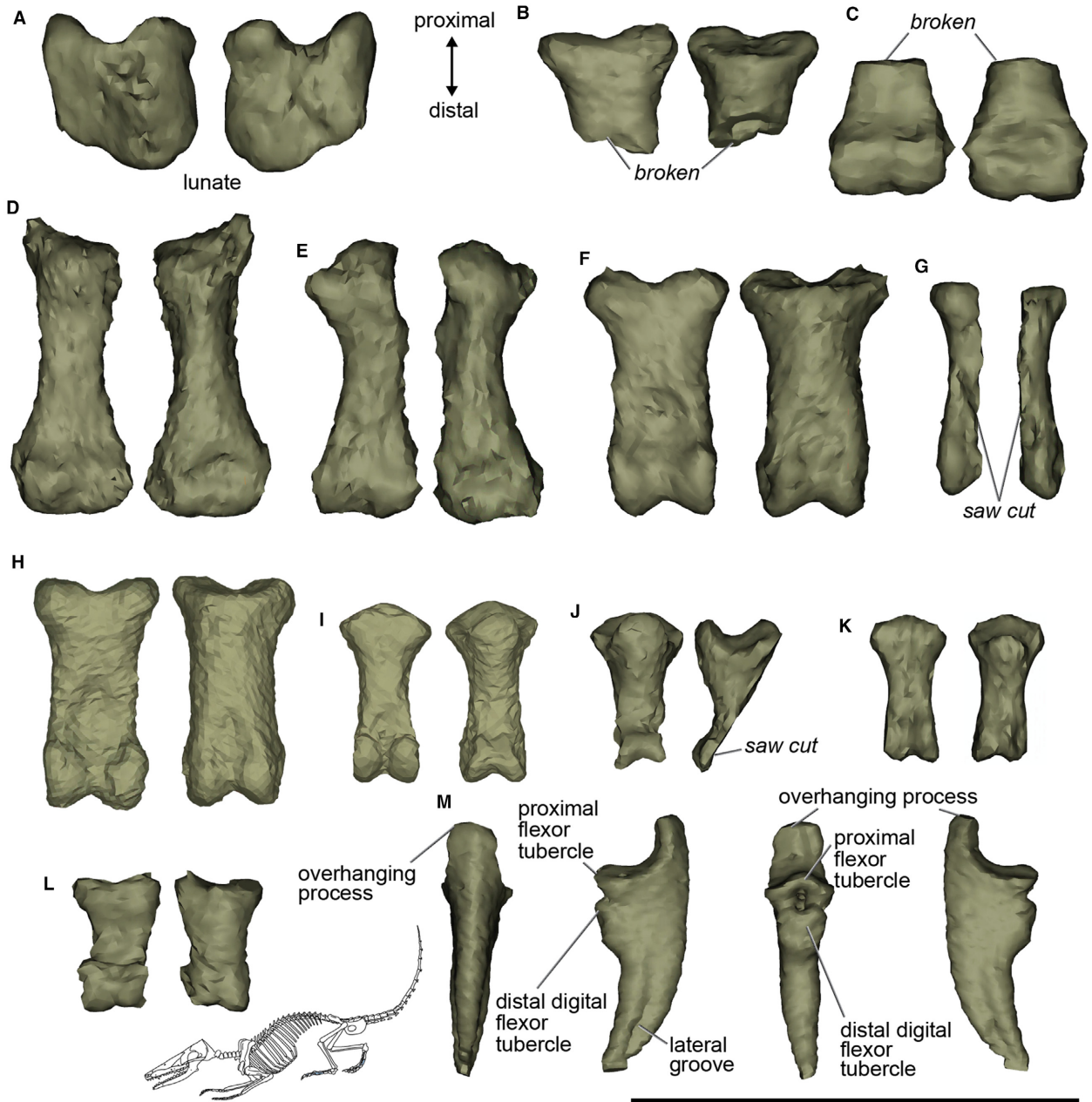


**FIG. 15.** Manus and pes elements of NMS G.2020.4.1.1, *Borealestes cuillinensis*. A, lunate. B–L, intermediate metacarpals/tarsals; M, ungula. A–L are shown in ventral (left) and dorsal (right) view; M in dorsal, medial, ventral and lateral view. Scale bar represents 5 mm.

clade to be more deeply nested within Docodonta (Fig. 4B). Taken together, these results suggest that the relationships within Docodonta may be more complex than anticipated, and that tree topology may change depending on available character partitions from cranium and skeleton, in addition to mandible and teeth. Without more cranial and postcranial material from key taxa from Russia and North America, it is difficult to resolve the topology of the clade more conclusively.

*Comparative anatomy and ecomorphological inference*

Examination of the two species of docodontan *Borealestes* (*B. serendipitus* and *B. cuillinensis*), finds little difference in their postcranial morphologies. Both are adult, as indicated by diagnostic features of their tooth eruption and dentaries (Panciroli et al. 2019, fig. 6; 2021a, fig. 7). In *Docodon victor*, which is known from a relatively complete growth series, the ultimate molar is positioned medial to the anterior

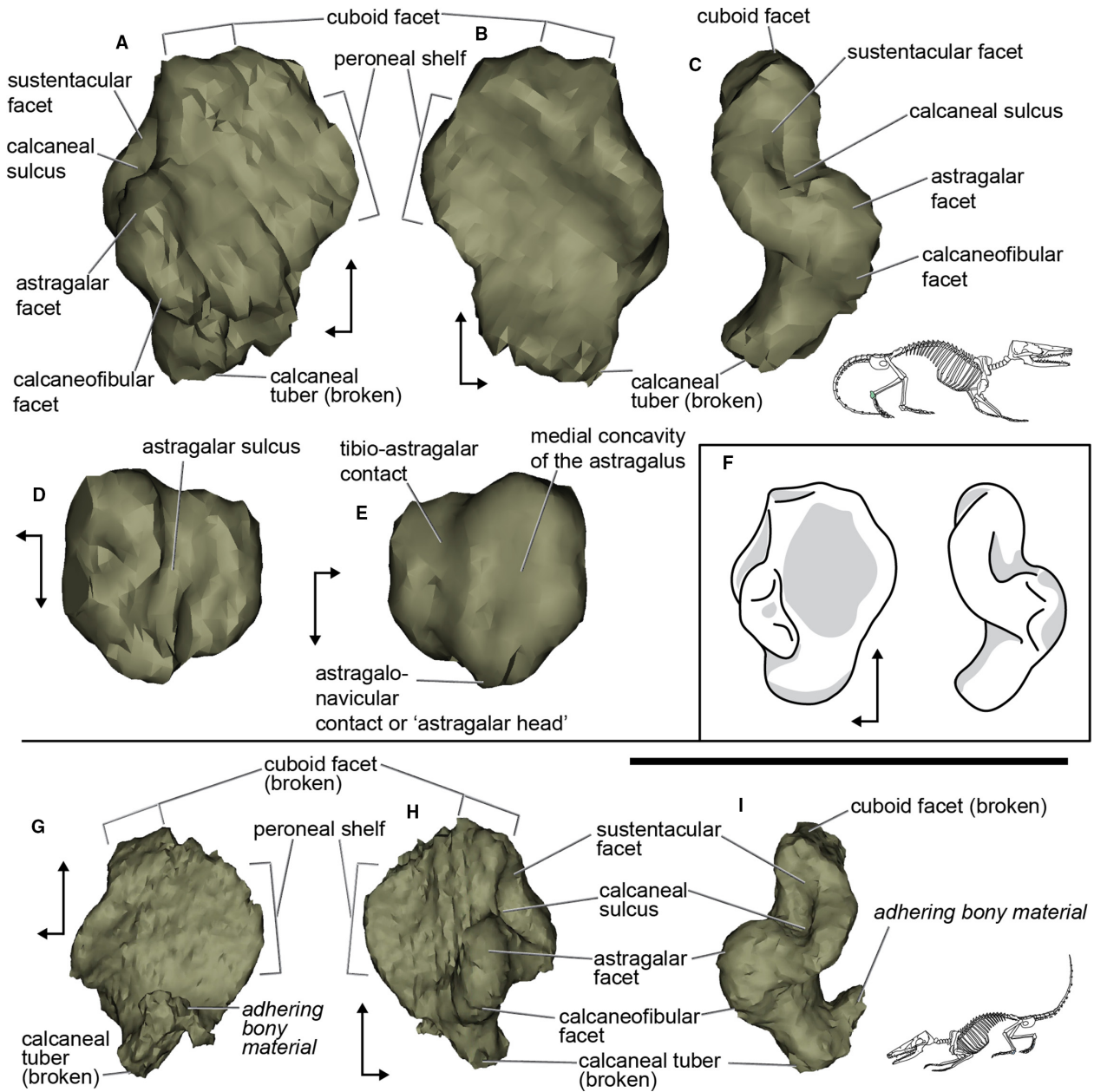


**FIG. 16.** Calcanea and astragalus of *Borealestes* species. A–C, NMS G.1992.47.121.1, *B. serendipitus*; A–C, right calcaneus: A, dorsal; B, ventral; C, medial view; D–E, right astragalus: D, ventral; E, dorsal view. F, composite outline drawing of *Borealestes* calcaneus. G–I, NMS G.2020.4.1.1, *B. cuillinensis*, left calcaneus: G, ventral; H, dorsal; I, medial view. Scale bar represents 5 mm.

part of coronoid process in juveniles, but in adults is shifted to a position anterior to the coronoid process, in alignment with the coronoid. In successively older adult individuals the coronoid shifts posteriorly as the mandible grows in length, resulting in a retro-molar space between the ultimate molar and the front of coronoid process (Schultz *et al.* 2017, fig. 4). In *Morganucodon* and docodontans, the ultimate lower molar of adults also has two roots closely compressed together or even confluent with each other (Kermack *et al.* 1973; Panciroli *et al.* 2019, 2021a). These

diagnostic adult features are present in specimens of *B. serendipitus* and *B. cuillinensis*, suggesting that they had reached adult stage.

The absence of epiphyses in most long bones and phalanges does not indicate a juvenile ontogenetic stage in mammaliaforms such as *Borealestes*. The adult limb bones of early-diverging mammaliaforms lack epiphyses even at early growth stages, as first observed in morganucodontans (Jenkins & Parrington 1976), and corroborated in almost all preserved limb elements of mature docodontans



(Martin 2005; Ji *et al.* 2006; Luo *et al.* 2015b; Meng *et al.* 2015). The single exception is found in the distal tibiae, which are sutured to the diaphysis in *Agilodocodon*, *Microdocodon* and *Docofossor*, probably related to a hypertrophied tibial malleolus hooked to the astragalus (Luo *et al.* 2015a; Zhou *et al.* 2019). The well-preserved long bones of *Haramiyavia* (Late Triassic) lack epiphyses (Luo *et al.* 2015a), and they are also absent among eutriconodontans, which are crown mammals (Jenkins & Schaff 1988; Ji *et al.* 1999; Martin *et al.* 2015; Chen *et al.* 2017). The absence of epiphyses in long bones and phalanges of *Borealestes* is therefore a plesiomorphic feature of mammaliaforms, which is retained in eutriconodontans.

Some other ossification-related traits of *Borealestes* species are also different to those crown-group mammals. In particular, the open suture of the acetabulum is shared with adult specimens of *Morganucodon*, *Castorocauda*, *Docofossor* and *Microdocodon*, as well as ontogenetically mature gobiconodontids. This is different to the fusion of the acetabular suture of the ilium, ischium and pubis in crown-group mammals. *Borealestes* and other stem mammals therefore show plesiomorphic features of skeletal fusion, different from most crown mammals including multituberculates, and stem and crown therians (Morris 1972; Kielan-Jaworowska & Gambaryan 1994; Chen & Luo 2013; Yuan *et al.* 2013).

Taken together, the proportions of the postcrania of *Borealestes* are intermediate between the more gracile docodontan taxa *Agilodocodon* (Meng *et al.* 2015) and *Microdocodon* (Zhou *et al.* 2019), and the more robust *Haldanodon* (Martin 2005) (Figs 7–16). *Borealestes* species also lack the extreme ecomorphological specializations seen in *Castorocauda* (Ji *et al.* 2006) or *Docofossor* (Luo *et al.* 2015a). The results of PCA on the postcrania of *Borealestes* species supports this observation (Figs 5, 6). Although there are indications that it was capable of scratch digging and swimming to some extent, both comparative morphology and principal component analyses suggest *Borealestes* species were non-specialist, lacking highly derived ecological or locomotor specializations or their associated morphologies.

The atlas neural arches of *Borealestes* species form part of the atlas–axis complex. Although the atlas centrum is not preserved in either specimen and the components of the atlas are not fused, the preserved halves of the arches suggest the atlas would have resembled that of other early mammaliaforms and cynodonts. The lack of fusion of components of the atlas is a plesiomorphic feature of cynodonts, similar to that seen in the tritylodontids such as *Oligokyphus* and *Kayentatherium* (Kühne 1956; Jenkins & Parrington 1976; Rowe 1988; Sues & Jenkins 2006). The vertebrae preserved in both *Borealestes* species suggest a similar morphology in the cervical and thoracic vertebrae to other docodontans, and to those of non-mammaliaform cynodonts (Sues & Jenkins 2006). In the caudal series of

*Agilodocodon* (Meng *et al.* 2015) there is a clear change in morphology from caudal 7 to caudal 8: the transverse process is reduced and the more posteriorly positioned vertebrae are more elongated. In *Microdocodon* (Zhou *et al.* 2019), this transition occurs from caudal 6 to caudal 7. Using *Agilodocodon* and *Microdocodon* for comparison, the single preserved proximal caudal in *Borealestes* is most likely to be from a position anterior to caudal 7–8, as the transverse processes of this caudal project quite far laterally. This projection is somewhat similar to that seen in *Castorocauda* (Ji *et al.* 2006), whereas in *Agilodocodon* the proximal caudal vertebrae are narrower and less flattened. The well-developed zygapophyses in *Agilodocodon* suggest a slender and probably more mobile tail than other docodontans, or other mammaliaforms such as *Megaconus* (Zhou *et al.* 2013, suppl. mat.) The single preserved proximal caudal of *Borealestes* appears to be intermediate between the morphologies of the proximal caudals of *Castorocauda* and *Agilodocodon* (Fig. 7N). The preserved distal caudals are similar to those in *Castorocauda*, which are essentially little changed from earlier mammaliaforms and even some tritylodontids such as *Oligokyphus* (Kühne 1956). We suggest a sturdy, but relatively mobile tail for *Borealestes*, supported by the presence of large chevrons which would have increased the dorsoventral depth and robustness of the tail. The isolated caudal vertebrae do not suggest a more specialized ecology in *Borealestes*.

No material from the posterior thoracic or lumbar regions is preserved in *Borealestes*. The reduction or loss of the lumbar ribs in mammaliaforms is variable among groups, even within subclades of mammaliaforms (Chen *et al.* 2017). For most docodonts for which the lumbar region is known, lumbar ribs of reduced size are retained. The exception is *Agilodocodon*, which has no lumbar ribs on the last four lumbar vertebrae, and shows a more distinctive thoraco-lumbar transition than *Castorocauda* (Meng *et al.* 2015). This can be interpreted to correspond to an increased range of movement in the posterior vertebral column. The ribs of *Borealestes* are preserved and resemble the morphology of most docodontans, showing no signs of the flattened, reinforced specialization for a semi-aquatic lifestyle seen in *Castorocauda* (Ji *et al.* 2006; Meng *et al.* 2015). However it is not possible to determine whether *Borealestes* had a distinctive thoraco-lumbar transition from the material preserved here.

In the geometric morphometric analysis, *Borealestes* was separated from extant taxa along PC3 in analyses of the humerus and ulna, but only the distal femoral articulation in the hind limb. This suggests that extant mammal forelimb shape may differ more significantly from that of early mammaliaforms like *Borealestes* than their hindlimb shape. However, this may instead be the result of the more extensive landmarking possible on the humerus and ulna of *Borealestes* (due to the relative completeness of

these elements), which may more effectively detect differences in bone shape between *Borealestes* and the extant taxa in our analysis.

The deltopectoral crest of the humerus of *Borealestes* species is flared and appears to be intermediate between the gracile arboreal *Agilodocodon* (Meng *et al.* 2015) and the robust semi-aquatic/digger *Haldanodon* (Martin 2005) and specialist digger, *Docofossor* (Luo *et al.* 2015a). This prominent deltopectoral crest would provide attachment for strong muscles (e.g. insertion of the pectoralis and deltoid muscles, and possibly also the origin of the brachialis muscle; Gambaryan *et al.* 2015) suggesting strength in the forelimb, particularly abduction and forelimb retraction. In *Haldanodon* the humerus is more robust than the femur. The shaft of the humerus is not preserved in NMS G.1992.47.121.1, however, comparing the morphology of the humerus in *B. cuillinensis* (Fig. 11E–H) with the femur in *B. serendipitus* (Fig. 13I–M), and looking at the morphology of the radius and ulna of these taxa (Fig. 12), these elements are all more gracile than those of *Haldanodon*, again suggesting a less robust morphology overall for *Borealestes*.

These observations are supported by the results of geometric morphometrics. The humerus of *Borealestes* is intermediate between the morphology of monotremes (*Ornithorhynchus*) and therians. They share negative scores, but the PC3 distance between *Borealestes* and therians is only slightly greater than between *Borealestes* and *Ornithorhynchus* (Fig. 6B). This captures a narrower radial and ulnar condyle in these taxa, and a larger, flared deltopectoral crest without clear distinction between the edges of the deltoid and pectoral crests (captured by SL2 and SL3). The proximal articular surface of the humerus is also much larger in *Borealestes* and *Ornithorhynchus*. The platypus, *Ornithorhynchus*, is often cited as an important taxon for understanding basal mammal postcranial morphology, due to the retention of some plesiomorphic characteristics such as a rigid pectoral girdle (Jenkins 1970). Although monotremes were previously cited as an example of a basal morphology for mammals (e.g. Isidro & Vazquez 2006) the majority of workers consider monotreme morphology and movement to be specialized and derived in its own right, and divergent from both extant therians (e.g. Jenkins 1970; Pridmore 1985; Gambaryan *et al.* 2002; Gambaryan & Kuznetsov 2013) and stem mammals discovered so far (e.g. Chen & Wilson 2015; Luo *et al.* 2015a; Meng *et al.* 2015). The similarity in humeral scores between these taxa may be linked to the more rigid pectoral girdle in both genera, and the position of the limbs (stance), which are not held under directly the body, as well as a shared capability at digging. Pridmore (1985) noted the complex movements of the humerus in *Ornithorhynchus*, which arcs and rotates considerably around the glenoid during propulsion; early

mammaliaforms may have exhibited similar forelimb movements. The more positive score in PC3 for *Borealestes* relative to *Ornithorhynchus*, and the distinct difference in the scores for the distal articulation of the femur in *Borealestes* from the rest of the dataset, suggests that *Borealestes* had a different posture than monotremes do today, and possibly a distinct hind limb movement that may not be comparable to any living mammal taxa.

The scapulacoracoid of *Borealestes* is not well preserved, but the portion that remains, including the coracoid, glenoid facet and ventral portion of the scapular blade, resembles that belonging to *Haldanodon* (Martin 2005). In the geometric morphometric analysis of the scapulacoracoid (scapula in the extant taxa), which is essentially restricted to the glenoid and position of the acromion, *Borealestes* scores similarly to *Tarsipes rostratus* (honey possum) (Fig. 6A). They share a narrower, elongate glenoid fossa that is more concave than in other taxa. *Ornithorhynchus* meanwhile, scores positively on this axis (PC3). Therefore although the monotremes may provide a useful data point for comparison with mammaliaforms such as *Borealestes*, the comparison is limited.

In *Haldanodon*, the proximal part of the ulna including the olecranon and articulation facets is approximately the same length as the rest of the ulna (Martin 2005, p. 228). This ratio is similar in *Docofossor*, which has an olecranon–ulna ratio of 47% (Luo *et al.* 2015a, suppl. mat.) and *Castorocauda* (Ji *et al.* 2006) but is not the case in *Microdocodon* (Zhou *et al.* 2019), which has an olecranon–ulna ratio closer to 28%. In *B. cuillinensis*, the ulna has an olecranon–ulna ratio of 32%, closer to those of *Microdocodon* and *Agilodocodon*. This would suggest that *B. cuillinensis* was neither a specialist digger nor swimmer based on the inferred ecologies for these taxa, although it is still above the 26% average olecranon–ulna ratio recorded in fossorial extant mammals (Chen & Wilson 2015). In the geometric morphometric analysis, the ulna of *Borealestes* plots near taxa that habitually swim (*Castor* and *Enhydra*) and dig with their forelimbs (*Oryzorictes* and *Euroscaptor* and to a lesser extent *Solenodon*) (Fig. 6C). They share a more developed olecranon process, and the proximal ulna is mediolaterally relatively wide medial to the articular surface of the olecranon. These morphologies are associated with enhanced muscular attachments for the forelimb to facilitate habitual digging and/or swimming motion. There is also a flange on the medial side of the olecranon (Fig. 12E, I), which is a feature commonly seen in extant mammals that are capable scratch diggers (Salton & Sargis 2008). The placement of *Borealestes* in relation to these taxa suggests that although not as specialized for fossorial or aquatic lifestyles as more ecologically derived docodontans like *Docofossor*, *Haldanodon* or *Castorocauda*, *Borealestes* was probably a capable digger and able to swim, similar to many small-bodied mammals today.

What remains of the ilium and ischium is similar to that seen in other docodontans, but with a slightly more developed iliac blade than in *Agilodocodon*, suggesting more muscle attachment in this area. The proportions of the manus can provide useful ecomorphological inferences among mammals, including mammaliaforms; for example, the proportion of proximal and distal metacarpals/tarsals can be informative, as can multivariate analyses incorporating all limb elements (Chen & Wilson 2015; Meng *et al.* 2017; Grossnickle *et al.* 2020). Unfortunately, only disarticulated scattered proximal and distal manus and pes elements are preserved in NMS G.1992.47.121.1. These elements resemble those in *Agilodocodon* (Meng *et al.* 2015), and are far less robust in morphology than those seen in the specialist digger *Docofossor* (which is also brachydactylous), or in *Haldanodon* (Martin 2005).

The *Borealestes* calcaneus does not resemble extant mammals, being closer to the morphology to other early mammaliaforms such as *Morganucodon*. It is slightly less elongate than in *Agilodocodon* and, perhaps surprisingly, less elongate than earlier tritylodontids such as *Oligokyphus* (Kühne 1956). The tibio-astragalar trochlea and post-astragalar shelf are less developed than in *Docofossor* (Luo *et al.* 2015a) and, as for the rest of the pedal and manual elements, there is no sign in *Borealestes* of the anatomical specializations for a fossorial lifestyle seen in *Docofossor*. The tibio-astragalar joint of the platypus, *Ornithorhynchus anatinus*, allows this semi-aquatic monotreme to abduct its feet relative to the limb, and provides a wide range of movement including eversion and hyperextension (Luo *et al.* 2015a). This appears to resemble the morphology of docodontan *Docofossor brachydactylus*, suggesting a similar posture and range of movement for this Jurassic fossorial taxon. The tibio-astragalar contact in *Borealestes* is shallow with a smaller astragalar head than in *Docofossor*, but the resemblance in morphology suggests that it would also have been able to abduct its feet relative to the limb, but less so than in *Docofossor*.

## CONCLUSION

The two species of docodontan *Borealestes* (*B. serendipitus* and *B. cuillinensis*) exhibit little difference in their postcranial morphologies. *Borealestes serendipitus* is larger and fractionally more robust than *B. cuillinensis*, as observable by comparing the humeri and manus and pes elements, but the difference is nominal. Both the observational analysis and principal components analysis support an interpretation of *Borealestes* species as ‘generalist’, that is, lacking derived ecomorphologies that would reflect the specialist behaviours that are clear in taxa such as *Docofossor* or *Agilodocodon*. But in some PCAs, *Borealestes* plots near extant mammalian scratch diggers and swimming taxa, supporting the interpretation that like many ‘generalist’ extant taxa

it was probably capable of both. The more abducted and laterally positioned limbs of *Ornithorhynchus* probably strongly influence its PCA scores, which places the platypus apart from extant therians in the PCA results (Figs 5, 6). Although there is some similarity in the results for the humerus in *Ornithorhynchus* and *Borealestes*, overall they do not occupy similar morphospace, so comparative similarity between them is limited. However, their placement in analyses of forelimb elements may reflect shared similarity in limb posture, and capacity for scratch digging and/or swimming. Results for the femur hint that hind limb posture and range of movement in *Borealestes* may not resemble that seen in any extant taxa.

The intermediate skeletal morphology of *Borealestes* postcranial morphology may be representative of the basal morphology of docodontans as a whole, which like many small mammals today includes a capability for scratch digging. Such morphology could have provided a blueprint that natural selection could then adapt into more specialized fossorial morphologies seen in the Late Jurassic docodontans (Martin 2005; Luo *et al.* 2015b). However, our phylogenetic analyses incorporating scores for postcranial characters return a novel topology compared to previous analyses using only dentomandibular characters, namely in the placement of *Borealestes* species as sister to a clade formed by *Agilodocodon* and *Microdocodon*. This separates them from the ‘basal docodontan’ clade previously formed to include (*Borealestes* + *Haldanodon* + (*Docofossor* + *Docodon*)). It suggests that interpretation of which taxa are ‘basal’ among docodontans may be more complex than anticipated. The derived position of *Borealestes* in our phylogenetic analysis stresses the necessity of including a wider sampling of postcranial characters for docodontans from outside China. This will not only help to resolve the clades’ relationships, but also reveal broader patterns of ecomorphological specialization in early mammals as a whole.

*Acknowledgements.* EP was funded during part of this research by grant number NE/L002558/1, then by the Leverhulme Trust and John Fell Fund. Additional funding came from the Palaeontographical Society and the Inverness Field Club. Fieldwork on the Elgol Coast SSSI was conducted with permission from the John Muir Trust, under permit from NatureScot. Thank you to all of the fieldwork teams who assisted with the collection of the specimens described herein. We acknowledge the European Synchrotron Radiation Facility for provision of synchrotron radiation facilities, and we would like to thank Paul Tafforeau for assistance in using beamline ID19. Thank you to Stephen Brusatte, Ian Corfe and Florian Fousseis for assistance in obtaining synchrotron beamtime. We would like to thank Tom Davies and Ian Butler for their time and expertise acquiring CT scans. We thank Roberto Portela-Míguez, Cody Thompson, Mathew Lowe and Robert Asher, Ben Marks and Adam Ferguson, and Andrew Kitchener and Zena Timmons for access to specimens of extant taxa. Funding for the acquisition of the extant mammal specimen data has been provided by the European Union’s Horizon

2020 research and innovation program 2014–2018 under grant agreement 677774 (European Research Council Starting Grant: TEMPO) to RBB. Sincere thanks to our reviewers, Thomas Martin and Lucas N. Weaver.

*Author contributions.* **Conceptualization** N Fraser, Z-X Luo, E Panciroli, S Walsh; **Data Curation** RBJ Benson, V Fernandez, A Martín-Serra, E Panciroli; **Formal Analysis** RBJ Benson, A Martín-Serra, E Panciroli; **Funding Acquisition** RBJ Benson, S Brusatte, N Fraser, E Panciroli, S Walsh; **Investigation** RBJ Benson, A Martín-Serra, E Panciroli; **Methodology** RBJ Benson, Z-X Luo, E Panciroli; **Project Administration** E Panciroli; **Resources** RBJ Benson, V Fernandez, N Fraser, E Panciroli; **Software** RBJ Benson, V Fernandez, M Humpage, A Martín-Serra, E Panciroli; **Supervision** RBJ Benson, N Fraser, Z-X Luo, S Walsh; **Validation** RBJ Benson, Z-X Luo, E Panciroli; **Visualization** M Humpage, E Panciroli; **Writing – Original Draft Preparation** E Panciroli; **Writing – Review & Editing** RBJ Benson, V Fernandez, N Fraser, Z-X Luo, A Martín-Serra, E Panciroli, S Walsh.

## DATA ARCHIVING STATEMENT

Scan data and 3D digital files are all available in the Morpho Source repository: <https://www.morphosource.org/projects/0000C1092>. Supporting information and data files are available in the Dryad Digital Repository: <https://doi.org/10.5061/dryad.5dv41ns5r>.

*Editor.* Lionel Hautier

## SUPPORTING INFORMATION

Additional Supporting Information can be found online (<https://doi.org/10.1111/pala.12577>):

- Appendix S1.** Body mass calculations.
- Appendix S2.** Geometric morphometrics.
- Appendix S3.** Phylogenetic analysis.
- Appendix S4.** Characters used in phylogenetic analysis.
- Appendix S5.** Phylogenetic analysis results.
- Appendix S6.** Principal components analyses.
- Appendix S7.** CT scan data DOIs.

## REFERENCES

- ADAMS, D. C., COLLYER, M. L., KALHONT-ZOPOLOU, A. and SHERRATT, E. 2017. geomorph: Geometric morphometric analyses of 2D/3D landmark data. R package v.3.0.5. <https://cran.r-project.org/web/packages/geomorph/index.html>
- AVERIANOV, A. O., MARTIN, T., LOPATIN, A. V., KRASNOLUTSKII, S. A. and IVANTSOV, S. V. 2010. New docodontans from the Middle Jurassic of Siberia and reanalysis of Docodonta interrelationships. *Proceedings of the Zoological Institute of the Russian Academy of Sciences*, **314**, 121–148.
- AVERIANOV, A. O., MARTIN, T., LOPATIN, A. V., SKUTSCHAS, P., SCHELLHORN, R., KOLOSOV, P. and VITENKO, D. 2018. A high-latitude fauna of mid-Mesozoic mammals from Yakutia, Russia. *PLoS One*, **13**, e0199983.
- BUDD, G. E. and JENSEN, S. 2000. A critical reappraisal of the fossil record of the bilaterian phyla. *Biological Reviews*, **75**, 253–295.
- BUTLER, P. M. 1997. An alternative hypothesis on the origin of docodont molar teeth. *Journal of Vertebrate Paleontology*, **17**, 435–439.
- CHEN, M. and WILSON, G. P. 2015. A multivariate approach to infer locomotor modes in Mesozoic mammals. *Paleobiology*, **41**, 280–312.
- CHEN, M. and LUO, Z.-X. 2013. Postcranial skeleton of the Cretaceous mammal *Akidolestes cifellii* and its locomotor adaptations. *Journal of Mammalian Evolution*, **20**, 159–189.
- CHEN, M., LUO, Z.-X. and WILSON, G. P. 2017. The postcranial skeleton of *Yanoconodon allini* from the Early Cretaceous of Hebei, China, and its implications for locomotor adaptation in eutriconodontan mammals. *Journal of Vertebrate Paleontology*, **37**, e1315425.
- DRYDEN, I. L. and MARDIA, K. 1998. *Statistical shape analysis*. Wiley, 496 pp.
- EVANS, H. E. and DE LAHUNTA, A. 2012. *Anatomy of the dog*. Elsevier, 872 pp.
- FEI VISUALIZATION SCIENCES GROUP 2015. Avizo Lite 9.0.1. FEI, Hillsboro, OR.
- FISH, F. E. 2000. Biomechanics and energetics in aquatic and semiaquatic mammals: platypus to whale. *Physiological & Biochemical Zoology*, **73**, 683–698.
- FOSTER, J. R. 2009. Preliminary body mass estimates for mammalian genera of the Morrison Formation (Upper Jurassic, North America). *PaleoBios*, **28**, 114–122.
- GABE, M., GASC, J. P., LESSERTISSEUR, J., SABAN, R. and STARCK, D. 1967. Mammifères: téguments et squelette. *Traité de Zoologie: Anatomie, Systématique, Biologie*, **16**, 1162.
- GAMBARYAN, P. P. and KIELAN-JAWOROWSKA, Z. 1997. Sprawling versus parasagittal stance in multituberculate mammals. *Acta Palaeontologica Polonica*, **42**, 13–44.
- GAMBARYAN, P. P. and KUZNETSOV, A. N. 2013. An evolutionary perspective on the walking gait of the long-beaked echidna. *Journal of Zoology*, **290**, 58–67.
- GAMBARYAN, P. P., ARISTOV, A. A., DIXON, J. M. and ZUBTSOVA, G. Y. 2002. Peculiarities of the hind limb musculature in monotremes: an anatomical description and functional approach. *Russian Journal of Theriology*, **1**, 1–36.
- GAMBARYAN, P. P., KUZNETSOV, A. N., PANYUTINA, A. A. and GERASIMOV, S. V. 2015. Shoulder girdle and forelimb myology of extant Monotremata. *Russian Journal of Theriology*, **14**, 1–56.
- GEISER, F. 1986. Thermoregulation and torpor in the kultarr, *Antechinomys laniger* (Marsupialia: Dasyuridae). *Journal of Comparative Physiology B*, **156**, 751–757.
- GINGERICH, P. D. 1973. Molar occlusion and function in the Jurassic mammal *Docodon*. *Journal of Mammalogy*, **254**, 1008–1013.

- GROSSNICKLE, D. M., CHEN, M., WAUER, J. G. A., PEVSNER, S. K., WEAVER, L. N., MENG, Q.-J., LIU, D., ZHANG, Y.-G. and LUO, Z.-X. 2020. Incomplete convergence of gliding-mammal skeletons. *Evolution*, **74**, 2662–2680.
- HILDEBRAND, M. 1985. Digging in quadrupeds. 89–109. In HILDEBRAND, M., BRAMBLE, D. M., LIEM, K. F. and WAKE, D. B. (eds). *Functional vertebrate morphology*. Belknap, 430 pp.
- HOPSON, J. A. and CROMPTON, A. W. 1969. Origin of mammals. 15–72. In DOBZHANSKY, T., HECHT, M. K. and STEERE, W. C. (eds). *Evolutionary biology*. Vol. 3. Appleton-Century-Crofts.
- ISIDRO, A. and VAZQUEZ, M. T. 2006. Phylogenetic and ontogenetic parallelisms on talo-calcaneal superposition. *The Foot*, **16**, 1–15.
- JANIS, C. M. and MARTÍN-SERRA, A. 2020. Postcranial elements of small mammals as indicators of locomotion and habitat. *PeerJ*, **8**, e9634.
- JENKINS, F. A. Jr 1969. Occlusion in *Docodon* (Mammalia, Docodonta). *Postilla*, **139**, 1–24.
- JENKINS, F. A. Jr 1970. Limb movement in a monotreme (*Tachyglossus aculeatus*): a cineradiographic analysis. *Science*, **168**, 1473–1475.
- JENKINS, F. A. Jr 1971. The postcranial skeleton of African cynodonts. *Bulletin of the Peabody Museum of Natural History*, **36**, 1–216.
- JENKINS, F. A. Jr and PARRINGTON, F. R. 1976. The postcranial skeletons of the Triassic mammals *Eozostrodon*, *Megazostrodon* and *Erythrotherium*. *Philosophical Transactions of the Royal Society B*, **273**, 387–431.
- JENKINS, F. A. Jr and SCHAFF, C. R. 1988. The Early Cretaceous mammal *Gobiconodon* (Mammalia, Triconodonta) from the Cloverly Formation in Montana. *Journal of Vertebrate Paleontology*, **8**, 1–24.
- JI, Q., LUO, Z.-X. and JI, S.-A. 1999. A Chinese triconodont mammal and mosaic evolution of the mammalian skeleton. *Nature*, **398**, 326–330.
- JI, Q., LUO, Z.-X., YUAN, C.-X. and TABRUM, A. R. 2006. A swimming mammaliaform from the Middle Jurassic and ecomorphological diversification of early mammals. *Science*, **311**, 1123–1127.
- KERMACK, K. A., MUSSETT, F. and RIGNEY, H. W. 1973. The lower jaw of *Morganucodon*. *Zoological Journal of the Linnean Society*, **53**, 87–175.
- KERMACK, K. A., MUSSETT, F. and RIGNEY, H. W. 1981. The skull of *Morganucodon*. *Zoological Journal of the Linnean Society*, **71**, 1–158.
- KERMACK, K. A., LEE, A. J., LEES, P. M. and MUSSETT, F. 1987. A new docodont from the Forest Marble. *Zoological Journal of the Linnean Society*, **89**, 1–39.
- KIELAN-JAWOROWSKA, Z. and GAMBARYAN, P. P. 1994. Postcranial anatomy and habits of Asian multituberculate mammals. *Fossils & Strata*, **36**, 1–92.
- KIELAN-JAWOROWSKA, Z., CIFELLI, R. L. and LUO, Z.-X. 2004. *Mammals from the Age of Dinosaurs: Origins, evolution, and structure*. Columbia University Press, 630 pp.
- KILBOURNE, B. M. 2017. Selective regimes and functional anatomy in the mustelid forelimb: diversification toward specializations for climbing, digging, and swimming. *Ecology & Evolution*, **7**, 8852–8863.
- KINDAHL, M. 1949. The embryonic development of the hand and foot of *Eremitalpa* (*Chrysochloris*) *granti* (Broom). *Acta Zoologica*, **30**, 133–152.
- KÜHNE, W. G. 1956. *The liassic therapsid Oligokyphus*. British Museum (Natural History), 149 pp.
- KÜHNE, W. G. and KRUSAT, G. 1972. Legalisierung des taxon *Haldanodon* (Mammalia, Docodonta). *Neues Jahrbuch für Geologie, Paläontologie und Mineralogie, Monatshefte*, **1972**, 300–302.
- LAI, P. H., BIEWENER, A. A. and PIERCE, S. E. 2018. Three-dimensional mobility and muscle attachments in the pectoral limb of the Triassic cynodont *Massetognathus pascuali* (Romer, 1967). *Journal of Anatomy*, **232**, 383–406.
- LILLEGRAVEN, J. A. and KRUSAT, G. 1991. Cranio-mandibular anatomy of *Haldanodon expectatus* (Docodonta; Mammalia) from the Late Jurassic of Portugal and its implications to the evolution of mammalian characters. *Contributions to Geology, University of Wyoming*, **28**, 39–138.
- LUNGMUS, J. A. and ANGIELCZYK, K. D. 2019. Antiquity of forelimb ecomorphological diversity in the mammalian stem lineage (Synapsida). *Proceedings of the National Academy of Sciences*, **116**, 6903–6907.
- LUO, Z.-X. 2007. Transformation and diversification in early mammal evolution. *Nature*, **450**, 1011–1019.
- LUO, Z.-X. and MARTIN, T. 2007. Analysis of molar structure and phylogeny of docodontan genera. *Bulletin of the Carnegie Museum of Natural History*, **39**, 27–47.
- LUO, Z.-X. and WIBLE, J. R. 2005. A Late Jurassic digging mammal and early mammalian diversification. *Science*, **308**, 103–107.
- LUO, Z.-X., MENG, Q.-J., JI, Q., LIU, D., ZHANG, Y.-G. and NEANDER, A. I. 2015a. Evolutionary development in basal mammaliaforms as revealed by a docodontan. *Science*, **347**, 760–764.
- LUO, Z.-X., GATESY, S. M., JENKINS, F. A., AMARAL, A. A. and SHUBIN, N. H. 2015b. Mandibular and dental characteristics of Late Triassic mammaliaform *Haramiyavia* and their ramifications for basal mammal evolution. *Proceedings of the National Academy of Sciences*, **112**, E7101–E7109.
- MACLEOD, N. and ROSE, K. D. 1993. Inferring locomotor behavior in Paleogene mammals via eigenshape analysis. *American Journal of Science*, **293-A**, 300–355.
- MARTIN, T. 2005. Postcranial anatomy of *Haldanodon expectatus* (Mammalia, Docodonta) from the Late Jurassic (Kimmeridgian) of Portugal and its bearing for mammalian evolution. *Zoological Journal of the Linnean Society*, **145**, 219–248.
- MARTIN, T. 2013. Mammalian postcranial bones from the Late Jurassic of Portugal and their implications for forelimb evolution. *Journal of Vertebrate Paleontology*, **33**, 1432–1441.
- MARTIN, T. 2018. Mesozoic mammals—early mammalian diversity and ecomorphological adaptations. 199–299. In ZACHOS, E. and ASHER, R. (eds). *Handbook of zoology: Mammalian evolution, diversity and systematics*. DeGruyter, 381 pp.
- MARTIN, T. and AVERIANOV, A. O. 2004. A new docodont (Mammalia) from the Middle Jurassic of Kyrgyzstan, central Asia. *Journal of Vertebrate Paleontology*, **24**, 195–201.



- MARTIN, T., MARUGÁN-LOBÓN, J., VULLO, R., MARTÍN-ABAD, H., LUO, Z.-X. and BUSCALIONI, A. D. 2015. A Cretaceous eutriconodont and integument evolution of early mammals. *Nature*, **526**, 380–384.
- MARTÍN-SERRA, A. and BENSON, R. B. 2020. Developmental constraints do not influence long-term phenotypic evolution of marsupial forelimbs as revealed by interspecific disparity and integration patterns. *The American Naturalist*, **195**, 547–560.
- MASCHENKO, E. N., LOPATIN, A. V. and VORONKEVICH, A. V. 2002. A new genus of the tegtotheriid docodonts (Docodonts, Tegtotheriidae) from the Early Cretaceous of West Siberia. *Russian Journal of Theriology*, **1**, 75–81.
- MENG, Q.-J., JI, Q., ZHANG, Y.-G., LIU, D., GROSSNICKLE, D. M. and LUO, Z.-X. 2015. An arboreal docodont from the Jurassic and mammaliaform ecological diversification. *Science*, **347**, 764–768.
- MENG, Q.-J., GROSSNICKLE, D. M., LIU, D., ZHANG, Y.-G., NEANDER, A. I., JI, Q. and LUO, Z.-X. 2017. New gliding mammaliaforms from the Jurassic. *Nature*, **548**, 291–296.
- MORRIS, P. 1972. A review of mammalian age determination methods. *Mammalian Review*, **2**, 69–104.
- NOWAK, R. M. 1999. *Walker's mammals of the world*. Johns Hopkins University Press, 1732 pp.
- PANCIROLI, E. and BENSON, R. 2021. New species of mammaliaform and the cranium of *Borealestes* (Mammaliformes: Docodonts) from the Middle Jurassic of the British Isles. *MorphoSource*. <https://www.morphosource.org/projects/0000C1092>
- PANCIROLI, E., SCHULTZ, J. A. and LUO, Z.-X. 2018. Morphology of the petrosal and stapes of *Borealestes* (Mammaliaformes, Docodonts) from the Middle Jurassic of Skye, Scotland. *Papers in Palaeontology*, **5**, 139–156.
- PANCIROLI, E., BENSON, R. B. J. and LUO, Z.-X. 2019. The mandible and dentition of *Borealestes serendipitus* (Docodonts) from the Middle Jurassic of Skye, Scotland. *Journal of Vertebrate Paleontology*, **39**, e1621884.
- PANCIROLI, E., BENSON, R. B. J., FERNANDEZ, V., BUTLER, R. J., FRASER, N. C., LUO, Z.-X. and WALSH, S. 2021a. New species of mammaliaform and the cranium of *Borealestes* (Mammaliformes: Docodonts) from the Middle Jurassic of the British Isles. *Zoological Journal of the Linnean Society*, **192**, 1323–1362. [doi:10.1111/zoo.1444](https://doi.org/10.1111/zoo.1444).
- PANCIROLI, E., BENSON, R. B. J., FERNANDEZ, V., HUMPAGE, M., MARTÍN-SERRA, A., WALSH, S., LUO, Z.-X. and FRASER, N. C. 2021b. Data from: Postcrania of *Borealestes* (Mammaliformes: Docodonts) and the emergence of ecomorphological diversity in early mammals. *Dryad Digital Repository*. <https://doi.org/10.5061/dryad.5dv41ns5r>
- POLLY, P. D. 2007. Limbs in mammalian evolution. 245–268. In HALL, B. K. (ed.) *Fins into limbs: Evolution, development, and transformation*. University of Chicago Press, 344 pp.
- PRIDMORE, P. A. 1985. Terrestrial locomotion in monotremes (Mammalia: Monotremata). *Journal of Zoology*, **205**, 53–73.
- R CORE TEAM. 2017. R: a language and environment for statistical computing. v.3.4.1. R Foundation for Statistical Computing, Vienna. <http://cran.R-project.org>
- REGNAULT, S., FAHN-LAI, P., NORRIS, R. N. and PIERCE, S. E. 2020. Shoulder muscle architecture in the echidna (Monotremata: *Tachyglossus aculeatus*) indicates conserved functional properties. *Journal of Mammalian Evolution*, **27**, 591–603.
- ROWE, T. 1988. Definition, diagnosis and origin of Mammalia. *Journal of Vertebrate Paleontology*, **8**, 241–264.
- SALTON, J. A. and SARGIS, E. J. 2008. Evolutionary morphology of the Tenrecoidea (Mammalia) forelimb skeleton. 51–71. In SARGIS, J. A. and DAGOSTO, M. (eds). *Mammalian evolutionary morphology*. Springer, 439 pp.
- SCHULTZ, J. A., BHULLAR, B. A. S. and LUO, Z.-X. 2017. Re-examination of the Jurassic mammaliaform *Docodon victor* by computed tomography and occlusal functional analysis. *Journal of Mammalian Evolution*, **26**, 9–38.
- SIGOGNEAU-RUSSELL, D. 2003. Docodonts from the British Mesozoic. *Acta Palaeontologica Polonica*, **48**, 357–374.
- SMITH, F. A., LYONS, S. K., ERNEST, S. K. M., JONES, K. E., KAUFMAN, D. M., DAYAN, T., MARQUET, P. A., BROWN, J. H. and HASKELL, J. P. 2003. Body mass of late Quaternary mammals. *Ecology*, **84**, 3402.
- SIMPSON, G. G. 1929. American Mesozoic Mammalia. *Memoirs of the Peabody Museum of Yale University*, **3**, 1–235.
- SUES, H.-D. and JENKINS, F. A. Jr 2006. The postcranial skeleton of *Kayentatherium wellsi* from the Lower Jurassic Kayenta Formation of Arizona and the phylogenetic significance of postcranial features in tritylodontid cynodonts. 114–152. In CARRANO, M. T. (ed.) *Amniote paleobiology: Perspectives on the evolution of mammals, birds, and reptiles*. University of Chicago Press, 448 pp.
- SWOFFORD, D. L. 2003. PAUP\*. Phylogenetic analysis using parsimony (\*and other methods). Version 4. Sinauer Associates, Sunderland, MA.
- SZALAY, F. S. 1994. *Evolutionary history of the marsupials and an analysis of osteological characters*. Cambridge University Press, 496 pp.
- WALDMAN, M. and SAVAGE, R. J. G. 1972. The first Jurassic mammal from Scotland. *Journal of the Geological Society of London*, **128**, 119–125.
- WEAVER, L. N. and GROSSNICKLE, D. M. 2020. Functional diversity of small-mammal postcrania is linked to both substrate preference and body size. *Current Zoology*, **66**, 539–553.
- YUAN, C.-X., JI, Q., MENG, Q.-J., TABRUM, A. R. and LUO, Z.-X. 2013. Earliest evolution of multituberculate mammals revealed by a new Jurassic fossil. *Science*, **341**, 779–783.
- ZHOU, C. F., WU, S., MARTIN, T. and LUO, Z.-X. 2013. A Jurassic mammaliaform and the earliest mammalian evolutionary adaptations. *Nature*, **500**, 163–167.
- ZHOU, C. F., BHULLAR, B.-A. S., NEANDER, A. I., MARTIN, T. and LUO, Z.-X. 2019. New Jurassic mammaliaform sheds light on early evolution of mammal-like hyoid bones. *Science*, **365**, 276–279.